National Library of Canada
Bibliothèque nationale du Canada

Canadian Theses Service
Service des thèses canadiennes

Ottawa, Canada
K1A 0N4

NOTICE

The quality of this microform is heavily dependent upon the quality of the original thesis submitted for microfilming. Every effort has been made to ensure the highest quality of reproduction possible.

If pages are missing, contact the university which granted the degree.

Some pages may have indistinct print especially if the original pages were typed with a poor typewriter ribbon or if the university sent us an inferior photocopy.

Reproduction in full or in part of this microform is governed by the Canadian Copyright Act, R.S.C. 1970, c. C-30, and subsequent amendments.

AVIS

La qualité de cette microforme dépend grandement de la qualité de la thèse soumise au microfilmage. Nous avons tout fait pour assurer une qualité supérieure de reproduction.

S'il manque des pages, veuillez communiquer avec l'université qui a conféré le grade.

La qualité d'impression de certaines pages peut laisser à désirer, surtout si les pages originales ont été dactylographiées à l'aide d'un ruban usé ou si l'université nous a fait parvenir une photocopie de qualité inférieure.

La reproduction, même partielle, de cette microforme est soumise à la Loi canadienne sur le droit d'auteur, SRC 1970, c. C-30, et ses amendements subséquents.

NL-339 (r. 88/04) c

Canada

National Library of Canada

Bibliothèque nationale du Canada

Canadian Theses Service

Service des thèses canadiennes

Ottawa, Canada
K1A 0N4

The author has granted an irrevocable non-exclusive licence allowing the National Library of Canada to reproduce, loan, distribute or sell copies of his/her thesis by any means and in any form or format, making this thesis available to interested persons.

L'auteur a accordé une licence irrévocable et non exclusive permettant à la Bibliothèque nationale du Canada de reproduire, prêter, distribuer ou vendre des copies de sa thèse de quelque manière et sous quelque forme que ce soit pour mettre des exemplaires de cette thèse à la disposition des personnes intéressées.

The author retains ownership of the copyright in his/her thesis. Neither the thesis nor substantial extracts from it may be printed or otherwise reproduced without his/her permission.

L'auteur conserve la propriété du droit d'auteur qui protège sa thèse. Ni la thèse ni des extraits substantiels de celle-ci ne doivent être imprimés ou autrement reproduits sans son autorisation.

ISBN 0-315-53210-6

Canada

Surface Scattering Using KeV Ions

by

Carolina Antonsen

Thesis submitted to the School of Graduate Studies of the University of Ottawa in partial fulfillment of the requirements for the degree of Master of Science in Physics

© Carólina Antonsen, Ottawa, Canada, 1989

UNIVERSITÉ D'OTTAWA
ÉCOLE DES ÉTUDES SUPÉRIEURES ET DE LA RECHERCHE

UNIVERSITY OF OTTAWA
SCHOOL OF GRADUATE STUDIES AND RESEARCH

PERMISSION DE REPRODUIRE ET DE DISTRIBUER LA THÈSE - *PERMISSION TO REPRODUCE AND DISTRIBUTE THE THESIS*

NOM DE L'AUTEUR* - NAME OF AUTHOR
ANTONSEN, Carolina

ADRESSE POSTALE - MAILING ADDRESS
906 - 2 Hanover Road
Brampton, Ontario L6S 4H9

GRADE - DEGREE
M.Sc. (Physics)

ANNÉE D'OBTENTION - YEAR GRANTED
1989

TITRE DE LA THÈSE - TITLE OF THESIS
SURFACE SCATTERING USING KeV IONS

L'AUTEUR PERMET, PAR LA PRÉSENTE, LA CONSULTATION ET LE PRÊT DE CETTE THÈSE EN CONFORMITÉ AVEC LES RÈGLEMENTS ÉTABLIS PAR LE BIBLIOTHÉCAIRE EN CHEF DE L'UNIVERSITÉ D'OTTAWA. L'AUTEUR AUTORISE AUSSI L'UNIVERSITÉ D'OTTAWA, SES SUCCESSEURS ET CESSIONNAIRES, À REPRODUIRE CET EXEMPLAIRE PAR PHOTOGRAPHIE OU PHOTOCOPIE POUR FINS DE PRÊT OU DE VENTE AU PRIX COÛTANT AUX BIBLIOTHÈQUES OU AUX CHERCHEURS QUI EN FERONT LA DEMANDE.

LES DROITS DE PUBLICATION PAR TOUT AUTRE MOYEN ET POUR VENTE AU PUBLIC DEMEURERONT LA PROPRIÉTÉ DE L'AUTEUR DE LA THÈSE SOUS RÉSERVE DES RÈGLEMENTS DE L'UNIVERSITÉ D'OTTAWA EN MATIÈRE DE PUBLICATION DE THÈSES.

THE AUTHOR HEREBY PERMITS THE CONSULTATION AND THE LENDING OF THIS THESIS PURSUANT TO THE REGULATIONS ESTABLISHED BY THE CHIEF LIBRARIAN OF THE UNIVERSITY OF OTTAWA. THE AUTHOR ALSO AUTHORIZES THE UNIVERSITY OF OTTAWA, ITS SUCCESSORS AND ASSIGNEES, TO MAKE REPRODUCTIONS OF THIS COPY BY PHOTOGRAPHIC MEANS OR BY PHOTOCOPYING AND TO LEND OR SELL SUCH REPRODUCTIONS AT COST TO LIBRARIES AND TO SCHOLARS REQUESTING THEM.

THE RIGHT TO PUBLISH THE THESIS BY OTHER MEANS AND TO SELL IT TO THE PUBLIC IS RESERVED TO THE AUTHOR, SUBJECT TO THE REGULATIONS OF THE UNIVERSITY OF OTTAWA GOVERNING THE PUBLICATION OF THESES.

March 10, 1989
DATE

Carleen Antonsen
(AUTEUR) SIGNATURE (AUTHOR)

* NB LE MASCULIN COMPREND ÉGALEMENT LE FÉMININ

F518-A525 85-12

UNIVERSITÉ D'OTTAWA
UNIVERSITY OF OTTAWA

UNIVERSITÉ D'OTTAWA UNIVERSITY OF OTTAWA

ÉCOLE DES ÉTUDES SUPÉRIEURES ET DE LA RECHERCHE

SCHOOL OF GRADUATE STUDIES AND RESEARCH

ANTONSEN, Carolina

AUTEUR DE LA THÈSE-AUTHOR OF THESIS

M.Sc. (Physics)

GRADE-DEGREE

DEPARTMENT OF PHYSICS

FACULTÉ, ÉCOLE, DÉPARTEMENT-FACULTY, SCHOOL, DEPARTMENT

TITRE DE LA THÈSE-*TITLE OF THE THESIS*

SURFACE SCATTERING USING KeV IONS

B. Hird

DIRECTEUR DE LA THÈSE-THESIS SUPERVISOR

EXAMINATEURS DE LA THÈSE-*THESIS EXAMINERS*

J. Hébert

B. Logan

R. Carnegie

(LE DOYEN DE L'ÉCOLE DES ÉTUDES SUPÉRIEURES ET DE LA RECHERCHE)

SIGNATURE

(DEAN OF THE SCHOOL OF GRADUATE STUDIES AND RESEARCH)

Abstract

Apparatus for scattering by keV ions, at grazing incidence angles, from atomically clean surfaces, was designed and assembled. An ultra-high vacuum chamber was equipped with a sample manipulator/goniometer and a rotating platform for mounting detectors, such as channeltrons. A combination bakeout oven/UHV chamber and differential pumping section support table was designed, constructed and tested. At the National Research Council, measurements to determine a cleaning procedure for Si(100) were performed. Ozonated samples were prepared and then, under ultra-high vacuum conditions, heated by electron bombardment and checked with AES and LEED. This information was used to define a cleaning procedure for Si(100) in the new ultra-high vacuum chamber, which does not yet have diagnostic surface probes. A single baking overnight can achieve pressures of 10^{-10} Torr; cleaning silicon successfully without checking with LEED or AES is possible.

Acknowledgements

I would like to express my sincere thanks to everyone in the Physics Department at the University of Ottawa, and the Microstructures Group at the National Research Council who aided and supported me in this work.

I would like to thank my supervisor, Dr. Brian Hird, who provided me with the unique opportunity to be the first aboard the new experimental program at the University of Ottawa.

I would like to thank Dr. R.A. Armstrong for his guidance and help, UHV chamber and silicon wafer sample holder. Many thanks to Drs. Tom Jackman, Mike Denhof and Brian Williams, also at the National Research Council.

Many thanks to Bob Hart, Ron, Herve, Len and Francois, for all the excellent machining, shop work and loan of their tools. Thanks go to Art Buser and Viorel Nicola of the electrical shop who taught me respect for high voltage circuits. My thanks also go to Ken and Charlie in Stores for expediting delivery of purchases and finding suppliers.

There are certain individuals without whom this thesis would not exist. I would like to thank S.A. Antonsen, whose financial support made it all possible.

Table of Contents

		Page
	List of Tables and Figures	vi
1.0	Introduction	1
2.0	Proposed Physical Measurements	4
2.1	Grazing Angle Incidence	4
2.2	Scattering Geometry	6
2.3	Ion Beam Requirements	8
2.4	Vacuum Requirements	9
2.5	Vacuum Interfacing	10
2.5.1	Pumping Requirements	10
2.5.2	UHV Pumps	13
2.6	Discussion of Options Possible	14
3.0	Experimental	19
3.1	Accelerator and Beam Line	19
3.2	I. Ion Acceleration and Mass Separation Section	20
3.3	Beam Line Sections II. and III: The UHV Apparatus	21
3.4	Vacuum Production	24
3.4.1	Laboratory Preparation	24
3.4.2	Roughing Line	25
3.4.3	Differential Pumping Section	25
3.4.4	The UHV Chamber	26
3.4.5	Accelerator and Beam Line	27
3.5	Scattering Geometry	28
3.5.1	Sample Position	28
3.5.2	Rotating Platform	29
4.0	Bakeout Oven	36
4.1	Introduction	36
4.2	Support Table and Oven Design	38
4.3	Oven Heaters	40
4.4	Test Baking	43
4.4.1	Lower Oven Calibration	43
4.4.2	Baking Procedure	44

Page

5.0 Sample Preparation for UHV 53
5.1 Sample Preparation at NRC 53
5.1.1 University of Ottawa Requirements 54
5.2 Electron Methods for Surface Analysis 55
5.2.1 LEED 55
5.2.1.1 LEED Experiment 56
5.2.1.2 Interpretation of LEED Data 56
5.2.2 Auger Electron Spectroscopy 58
5.3 Experimental 60
5.3.1 Ozonated Silicon Wafer 62
5.4 Sample Measurements 64
5.4.1 Argon Bombarded Si(100) 64
5.4.2 First Ozone Treated Sample 66
5.4.3 Second Sample 68
5.4.4 Third Sample 68
5.4.5 Fourth Sample 70
5.4.6 Summary of Sample Measurements 71
5.4.6.1 Temperature Measurement 72
5.4.7 Surface Structure from LEED 73
5.4.8 Reappearance of Contaminants 75

6.0 Conclusions 91
6.1 Conditions for Clean Si(100) 91
6.2 Baking Procedure 92
6.3 Surface Scattering Experiment Considerations 93

References 95

List of Tables and Figures

		Page
Figure 2.1	Detection System Schematic	17
Figure 2.2	Slit Width Geometry	18
Figure 3.1	Beam Line	31
Figure 3.2	Second 0.5mm Slit	32
Figure 3.3	Target Chamber	33
Figure 3.4	Schematic of Roughing System	34
Figure 3.5	The Rotating Platform	35
Figure 4.1	The Two-Height Table	46
Figure 4.2	Top View of Bakeout Oven Showing UHV Apparatus	47
Figure 4.3	The Controller Circuit	48
Figure 4.4	"Lower" Oven Calibration	49
Figure 4.5	"Upper" Oven Bake	50
Figure 4.6	"Upper" Oven Bake #2	51
Figure 4.7	"Lower" Oven Bake	52
Figure 5.1	LEED Configuration at NRC	76
Figure 5.2	Cylindrical Mirror Analyzer	77
Figure 5.3	Electron Energy Diagram	78
Figure 5.4	Sample Mounting Configuration	
	a) Sample Holder/Electron Bombarder Block	79
	b) Sample Mounting Plate	80
Figure 5.5	Electron Bombarder Circuit	81
Figure 5.6	Auger Spectrum of Zeroth Sample	82
Figure 5.7	Initial Auger Spectra of Sample No. 1 Showing Presence of SiO_2	83
Figure 5.8	Auger Spectrum of Clean Surface (No. 3)	84
Figure 5.9	Spatial Distribution of Contaminants C and O.	85
Table 5.1	Summary of Sample Cleaning Measurements	86
Figure 5.10	Temp. I.R. vs. Temp. D.F. Comparing Pyrometer Readings	87
Figure 5.11	Relation between Power and Temperature	88
Figure 5.12	Ewald Sphere Construction	89
Table 5.2	Reappearance of Contaminants	90

All tables and figures are found following their corresponding chapters.

Surface Scattering Using keV Ions

1.0 Introduction

There is a history of ion- surface collisions. The first publications on ion scattering as a tool for surface composition date back to 1959 (1). The availability of commercial ultrahigh vacuum equipment, allowing atomically clean surface conditions, sparked renewed interest in ion-surface collisions and in surfaces (2).

Ultrahigh vacuum (UHV) is defined as pressure less than 10^{-9} torr (3). The necessity of ultra- high vacuum for studies of well-defined surfaces follows from the kinetic theory of gases which predicts a monolayer of molecules can be adsorbed in about 1 second at a pressure of 10^{-6} torr (4).

One technique increasingly applied since the 1970's to surface composition and interaction investigations has been Rutherford backscattering (5,6). However, at low energies ($\leq$ 5keV) neutralization effects became problematic (e.g. with an electrostatic energy analyzer). Scattering yields appeared to result from both neutralization and beam attenuation inside the target (7).

Rutherford backscattering has also been combined with shadowing and blocking techniques to determine specific target surface structures, such as in MEIS (Medium Energy Ion Scattering) (8,9). Low energy techniques such as ICISS (impact collision ion scattering spectroscopy) detect the ions backscattered along their incident trajectories (often at grazing

incidence), so that blocking is negligible (10). Even so, the detection of neutral atoms, in addition to scattered ions, was recommended for improved determination of surface reconstruction and relaxation (11).

Ion- thin foil interactions were set up to measure charge state fractions (12,13), and attributed to inner shell vacancy production and surface neutralization. Measurements for backscattered ions agreed closely with results for particles traversing thin foils (13).

Recently H. Winter et al. have been using grazing incidence angles to investigate polarized light emitted from surfaces. This observation was correlated with the occurrence of ion neutralization at the specular reflection angle (14), which occurred in different proportion than for ion- tilted foil interaction. It was described in terms of a two-step process:

(i) the incoming ion is first polarized in the field of the surface, and

(ii) level excitation or electron transfer occurs.

The present apparatus is being set up to look at ion-surface interactions at grazing incidence by detection of the forward scattered particles. Initially, charge state fractions at the specular reflection angle will be measured. This will complement the laboratory's function of studying ion-single atom collisions. Parameters to be studied can include element to element variations and surface effect variations involving work function and absorbate coverage which affect ion yields.

This thesis will give a description of the construction of (new) apparatus for ion-surface collisions under ultrahigh vacuum conditions.

The UHV system design was partially based on the apparatus that was in successful operation at the AECL Chalk River Nuclear Laboratories (15). The design considerations and option selections will be discussed, including ion beam requirements, vacuum requirements and vacuum interfacing with an existing 10^{-6} torr beam line, and the effect of the system's constraints on the initialization of the experimental program.

The design, implementation and testing of a bakeout oven, capable of enclosing the entire UHV apparatus section, is reported. Baking results in accelerated desorption of water vapour and other gases from all internal surfaces, necessary for the achievement of ultrahigh vacuum conditions.

Measurements to delineate a method for sample preparation (without measuring its condition) will be described and analyzed. The investigation of the UV ozone surface cleaning method, for Si(100), was performed at the National Research Council. The removal of the contaminants (oxygen and hydrogen) was monitored using LEED (Low Energy Electron Diffraction) and AES (Auger Electron Spectroscopy). Silicon was chosen as a target material primarily because of its easy cleaning abilities.

2.0 Proposed Physical Measurements

2.1 Grazing Angle Incidence

High energy ion scattering, at grazing angle incidence, is a surface effect. A strong peak in the intensity of the scattered particles, the ions and neutralized atoms, at the specular reflection angle, was measured by H. Winter et al. (14): for grazing incidence ions, from a clean flat polycrystalline surface. The strong peak is a surface effect, since the directional properties of the solid determine the alignment of the scattered ion or atom. Any directional properties of a polycrystalline metal are lost, a few atomic layers into the bulk. As well, on reducing the angle of incidence, the upper limit of the range of scattering angles, due to blocking effects, decreases, such that the reflected beam contracts to directions around specular (16).

Grazing incidence is a surface technique which depends on the alignment of the surface and depends on surface roughness. Optical radiation from keV ions scattered at a monocrystalline surface, at grazing incidence, shows a strong dependence on surface crystallography and the cleanness of the surface (17). The angular distribution due to violent collisions are reduced for ions specularly reflected from an absolutely clean and flat surface (14).

For atomic collisions in the keV range the force of interaction between two colliding particles is almost wholly repulsive and usually believed to be of the screened Coulomb type (16). For fast ions,

interpretations are in terms of a two-step process:

(i) collisional excitation in the close vicinity of the surface, and

(ii) resonant electron transfer from (to) the non-localized states in the conduction (valence) band to (from) the ion.

The first step is attributed to the total energy $\bar{E}$ of the incoming ions, in the second step, the normal component of $\bar{E}$ (with respect to the surface) is responsible for both short-range Auger -neutralization and -de-excitation, and long-range resonance -ionization and -neutralization (14). There is evidence supporting a model of the formation of the excited state way above the surface layer (18).

The scattering model is quite similar to the theories in ion- single atom collisions. Level degeneracies which are important in the level crossing theories of ion- atom scattering probably account for the element- to- element variations. Level degeneracies depend on the critical internuclear distance for a given pair of atoms and the effective range over which electron promotion takes place. The relative position of the Fermi-level, with respect to the binding energy of the level of the atom, is the crucial parameter (14) determining the direction of the resonant electron transfer.

2.2 Scattering Geometry

It is the intent of this experimental program to investigate ion neutralization at grazing angle incidence. At first, the preferred detector location will encompass a range of angles surrounding the specular reflection angle. The task, at grazing incidence, for small angles of detection, will be in separating the reflected beam from the background, produced by those ions missing the target. This condition will occur for collimated ions, whenever the target size, as "seen" by the incident beam, is reduced smaller than the beam width, by sample rotation towards smaller angles of incidence. For 10° incident ions, H. Akazawa et al. (19) were able to arrange a microchannel plate so that the incident beam hit the lower edge and reflected ions between 0° and 24° could be detected.

Unlike surface lattice structure determination techniques, a random surface orientation, rather than a channeling direction, is preferred. Channeling has been described as when ions, travelling along an aligned direction, are seen to make a gentle oscillatory motion around the centre of the crystal channels without coming close to the surrounding atomic strings, and thus able to travel microns deep into the crystal (9). Channeling occurs if the incident ions start close to the channel axis and if they have an angle less than the critical angle with the channel axis. An ion can escape from the channel if the energy in the transverse motion is larger than the channel barrier energy. However, at high particle energies the probability of channelling is negligible (20).

Another surface focussing effect affecting yields is surface "semi-channeling". Semi-channels are only present when the atomic rows of the second layer are situated between the atomic rows of the first layer. This occurs, for example, when the incidence plane is chosen parallel to one of the <110> directions lying in the (100) face of an fcc crystal, contributing to the total reflected yield (16).

2.3 Ion Beam Requirements

It is known the velocity of the incident ions affect the transition probability for an electron transfer. The relevant parameter governing the ion- surface interacton is the perpendicular velocity of the ion with respect to the surface, as opposed to the motion parallel to the surface (21,22). The parallel velocity component seems to place an important role, more for low energy incident ions. J.N.M van Wunnik et al. (23) measured a maximum for the negatively charged fraction of incident H^+ ions (angle 80°) on cesiated tungsten (work function 2.15eV) for decreasing parallel velocities, beginning at 2keV.

As well, the ion dose must be kept low enough so damage to the sample is minimized. Graser and Varelas (17), for 70 - 200keV He^+ ions incident at grazing angle on monocrystalline (110) NiFe, kept the ion beam dose below 4×10^{15} ions/cm^2. In the present case, assuming an absolute maximum beam current of 10^{-6}A for a 1mm beam diameter, the dose would not exceed 8×10^{14} ions/cm^2/s at normal incidence.

The present ion beam is capable of producing ions from ~~approximately~~ 10keV to a maximum of 150keV. The facility is able to produce both positive and negative ions of various elements. As yet, there has been no investigation of charge transfer between incident negative ions and surfaces.

Collimation of the ion beam is important for grazing angle experiments. A 1.3mm beam width at the target will produce a spot size of 25mm on the sample for an angle of incidence of 3°.

2.4 Vacuum Requirements

Meaningful experiments are best accomplished on surfaces in a chemically pure and monocrystalline state. For example, the amount of coverage on a surface effects changes to the work-function of a surface (23,24). Clean surfaces are best maintained by minimizing adsorption onto the surface via an ultrahigh vacuum environment. Even so, measurements are often done as a function of surface cleanliness (17).

An ultrahigh vacuum environment is also beneficial for efficient target cleaning. Extra outgassing from the target is expected when it is sputtered with ions or heated.

At a background pressure of 2 X 10^{-10} mbar (1.5 X 10^{-10} torr), assuming a sticking coefficient of unity, 0.1 monolayers are adsorbed 15 min. after cleaning (17). Actual sticking probabilities are much lower than unity for various materials. It has been estimated the initial sticking probability for O_2 molecules on clean Si(110) is 6 X 10^{-3}, and on Si(100) is 3 X 10^{-2} (25).

2.5 Vacuum Interfacing

2.5.1 Pumping Requirements

The problem of connecting a "dirty" 10^{-6} torr accelerator to an ultrahigh vacuum system has been successfully tackled by previous workers (1,2,15). They included one or more intermediate chambers between the two extreme vacuum regions to act as a vacuum buffer. The resulting sections were kept separate by small apertures or narrow pipes; each section was kept evacuated by its own pumps.

The decision had been made that the apertures separating the vacuum sections would double as slits for the ion-optical system. It was felt one differential pumping section would suffice.

Regions of 5×10^{-11} torr, 10^{-9} torr and 10^{-6} torr, separated by 1mm slits, were planned. The pumping requirements for each region were calculated as follows.

The number of molecules which cross a surface, per square meter, per second, is equivalent to the number of collisions against a wall, such that

$$n_x \,/m^2/s = {}^1/_4\, n\, \bar{v}$$

n is the molecular density (here, the total number of molecules per m^3) and $\bar{v}$ is the mean velocity (26). The number of molecules crossing a slit of area A is therefore $n_x A$. Here $\bar{v}$ is the mean velocity of air at room temperature = 460 m/s.

The molecular density at a pressure P_o (torr) is

$$n = \frac{N_A}{22.4} \times \frac{P_o}{760}$$

where $N_A = 6.02 \times 10^{23}$ is Avogadro's number, 760 torr is the standard pressure, and 22.4 l is the volume of 1 mol at standard temperature and pressure. At 10^{-6} torr, n is 3.5×10^{13} molecules per litre.

The flow rate through an aperture of area A is

$$n_x = \frac{1}{4} \frac{N_A}{22.4} \frac{P_o}{760} \bar{v} A$$

molecules/s. The molecular crossing rate, from the 10^{-6} torr to the 10^{-9} torr region, through the first 1mm slit, is therefore 3.2×10^{12} molecules per second. This is a volume flow rate, as measured in terms of P_o, the pressure on the high pressure side of the aperture. Hence

$$S_o = {}^1/_4 \, \bar{v} \, A$$

where the quantity S_o, in units of volume/time, is defined as the conductance, and is independent of P_o. This becomes

$$S_o = 11.5 \frac{\pi d^2}{4} \text{ litres/s}$$

for an aperture of diameter d centimetres.

The gas, that flows into the lower pressure region P_1 from the region P_o, expands proportionally such that the volume flow rate in P_1 is

$$S_1 = {}^1/_4 \, \bar{v} \, A \frac{P_o}{P_1}$$

For a 1mm diameter aperture the conductance $S_o = 0.09$ l/s. For the same aperture, the conductance S_1, into the region $P_1 = 10^{-9}$ torr, from $P_o = 10^{-6}$ torr, is 90 l/s, since the

pressure P_1 is 1000 times less than P_o. Similarly, for a second 1mm aperture, the conductance into the 5×10^{-11} torr region, from the 10^{-9} torr region, is 1.8 $l/_s$.

The pressure in the intermediate region may be higher than 10^{-9} torr due to the high gas load from the 10^{-6} torr region, and consequently there may be a slightly higher gas load on the UHV region. It is worth considering, if the intermediate region had only a vacuum corresponding to 10^{-8} torr, then the required pumping speed is increased to 18 $^l/_s$.

Assuming the emission of particles passing through both slits is uniform in all directions, a fraction of the particles from the 10^{-6} torr region will cross into the 5×10^{-11} torr region. This would be the solid angle fraction of the 3.2×10^{12} particles per second leaking into the 10^{-9} torr region, at the second slit. The solid angle of the second slit at the first depends on the length between the two slits. Hence

$$n_f = \frac{A/L^2}{2\pi \text{ steradian}} \times 3.2 \times 10^{12}$$

where n_f is the solid angle fraction, A the area of the second slit, and L the distance between the two slits. n_f is negligible compared to the leak rate of 3.2×10^9 particles per second, for L > 0.4m. For slits separated by 1m, n_f is 4.0×10^5 particles per second.

Other factors also contribute to the total leak rate. These include the outgassing of the vacuum envelope and the equipment therein, as well as the temporary presence of the ion beam. For a beam current of 10^{-11}A, there are $10^{-11} / 1.6 \times 10^{-19} = 6 \times 10^7$ ions$/_s$ entering into the UHV region, requiring an additional $0.02^l/_s$ of pumping. A stainless steel envelope, baked at 400°C for 12h, will outgas at 10^{-12} Torr litres s^{-1} cm^2 (2,3).

2.5.2 UHV Pumps

A description of pumps able to evacuate apparatus to the UHV range has been compiled by Hobson (3): diffusion pumps, ion pumps, getter pumps, turbomolecular pumps and cryopumps. Advantages and disadvantages of these pumps, pertaining to the design of the present experiment, will be briefly discussed.

Ion pumps provide 100% clean pumping. However, ion pumps have limits to the total gas which they can pump. It is necessary to bake the ion pump regularly in order to avoid noble gas instability i.e. when the pump gives off already pumped noble gases. A standard system of 5 ion pumps on a UHV chamber gives a pumping speed of 200 l/s (Varian VacIon literature). Getter and cryopumps also have limits to the total gas which they can pump.

Both oil-diffusion and turbomolecular pumps have a high throughput and require only a short pumping down time. They are capable of removing significant amounts of gas from the system indefinitely. However, turbomolecular pumps suffer from mechanical vibration, and must be isolated so as not to disturb any experimental alignments. With diffusion pumps, liquid nitrogen cold traps are required. There may be hydrocarbon or other contaminant backstreaming.

An Edwards E04 diffusion pump and VG CCT100 liquid nitrogen cold trap were already available in the laboratory. A combined pumping speed of 300 l/s made this a reasonable choice for the differential vacuum region. A diffusion pump/cold trap combination was also chosen for the UHV region. Also included was a titanium sublimation pump to getter the outstanding contaminants prior to each experiment.

2.6 Discussion of Options Possible

A standard stainless steel chamber, with an inside diameter of 293mm, delimited the UHV region. The centre of the chamber, at the focus of all the ports, was reserved for the target location. Two options were originally proposed for the scattered particle analysis. One option utilized the laboratory's high resolution $\pi/\sqrt{2}$ electrostatic analyzer. The second option employed a low resolution charge separator.

An electrostatic analyzer (E.S.A.) is an energy/charge filter. An E.S.A. at a particular voltage setting can accept only ions of the same E/q. Neutrals are not detected. Electrostatic analyzers have been used in conjunction with the time-of-flight (T.O.F.) technique (7,27,28). In this technique, the incoming ion beam is controlled by a pulse generating system. A time- to- pulse height converter measures the scattered ions' flight time through the E.S.A., such that the ions with different ratios m/q can be separated. For the present experiment, T.O.F. would identify which ions were, in fact, the reflected ones.

The possibility of an ion beam pulsing system had been examined. Two deflecting plates with sufficient voltage could be oscillated on and off. 30ns resolution of a multichannel pulse height analyzer was required to distinguish adjacent masses, where

$$\Delta T = \text{Flight Time}_{m2} - \text{Flight Time}_{m1},$$

for $m_1 = m_2 - 1$ a.m.u. This criterion affected the length, separation and voltage requirements of the deflecting plates. The time resolution criterion also affected the minimum flight path length, d_{min}, such that

$$d_{min} = \Delta T \sqrt{2E/m} \ .$$

The size of the sample chamber was a severe restriction. The laboratory's E.S.A. did not fit inside the sample chamber, thus it was not possible to do energy analysis of the scattered ions inside the chamber. Mounting the E.S.A. outside the chamber would have required differentially pumping the entrance slit to the analyzer. It would have also have restricted the detecting apparatus to the range of angles allowed by its fixed port location.

Therefore it was decided to do charge fraction measurements. For a detection system to be mounted within the chamber, it had to be located at least 40mm from the sample and also lie within the chamber's 146mm radius. (The 40mm constraint was necessary to allow sufficient space for sample manipulation.) A low resolution charge separator could be designed to fit within this length constraint. The big advantage of mounting the detectors within the chamber was the large range of angles available for study, without port restrictions. A rotating platform on which to mount the detectors was consequently designed and constructed (Section 3.5) The charge separator, as conceived, was to consist of 3 channeltron electron multipliers, located side-by-side, with their apertures along an arc, behind one set of deflecting plates. The potential between the plates would cause positive ions to be deflected towards the negative plate and one of the three channeltrons; neutrals would not be deflected and would collide with the central channeltron; negative ions would be deflected towards the positive plate and the third channeltron. A schematic description of the planned detection system is given in Figure 2.2. Similar charge separators have been used previously, in the

laboratory's gas target studies.

A set of antiscattering slits would be required in order to reduce the incidence of stray ions onto the detectors. Two locations had been discussed: 1. opposite the sample face, and 2. in the path of the ion beam preceding the sample. For the second option, the antiscattering minimum slit width w would be equivalent to the diameter of a cone, formed by the crossing of the paths most divergent, of two ions, passing through the two slits of diameters d_1 and d_2 (Figure 2.3), such that

$$w = \frac{(d_1 + d_2)\,x}{L} + d_2$$

where L is the distance between the slits, and x the distance from d_2 to the antiscattering slits.

Figure 2.1 Detection System Schematic

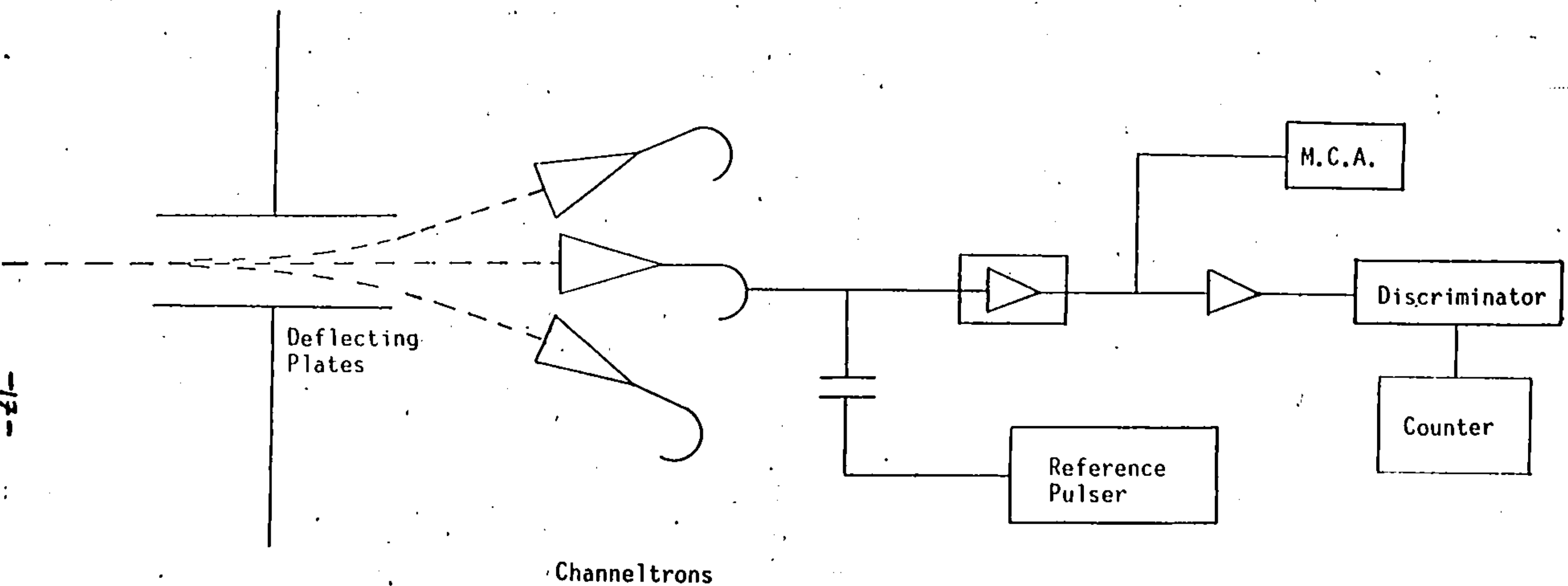

Figure 2.2 Slit Width Geometry

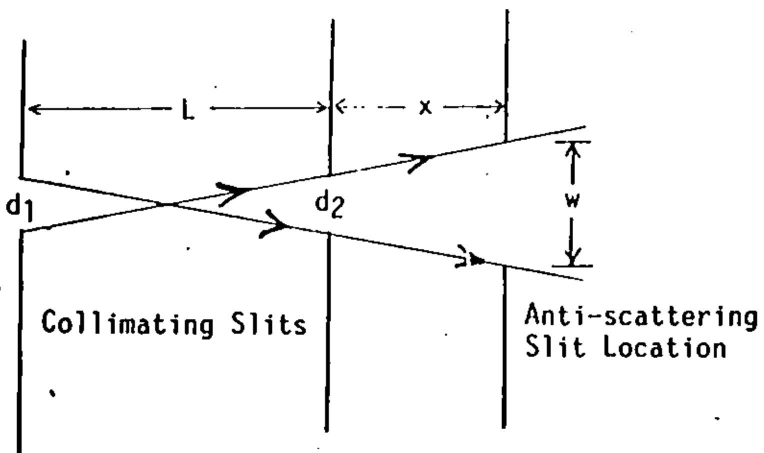

3.0 Experimental

3.1 Accelerator and Beam Line

The apparatus for the present experiment comprises three beam line sections, each section to be operated at separate baseline pressures:

I. Ion Acceleration and Mass Separation Section, at 10^{-6} torr

II. Differential Pumping Chamber, at 10^{-9} torr

III. Target Chamber, at ultrahigh vacuum.

A diagram of the beam line is given in Figure 3.1. The beam line sections II and III are both constructed of UHV- compatible apparatus: both sections are necessary in order to achieve ultrahigh vacuum in the vicinity of the sample. Two slits of 0.5mm diameter 1 m apart have been designed to divide I. from II. and II. from III. They will also act as collimation slits for the ion beam.

Ions for this experiment are produced by a 150 keV accelerator supplied by a Danfysik 911A ion source. This is a hollow cathode, hot filament arc source specially designed to operate with a wide range of vapour pressure materials. It is therefore able to produce beams of a wide range of elements, from 5 to 150 keV. In previous experiments, Mg, Na, Li and I ions were produced (29). Current is on the order of 10^{-8} A and up to 10^{-6} A for some ions. For the present application, hydrogen ions are proposed; ions with small mass such as hydrogen or helium would inflict less damage on the sample.

Mass separation is accomplished with a 30° deflection magnet. The

beam is to be aligned for fine adjustments with two steering magnets, one on either side of the mass-separating magnet. The steerers produce a weak, uniform field over a 20cm length of the beam, which deflects the beam slightly (but has negligible effect on its focussing properties).

Precise collimation will be accomplished with the two 0.5 mm slits 1 m apart, and an antiscattering slit another 75 mm further downstream, just inside the sample chamber. The 0.5mm slits have been designed to be electrically isolated from the stainless steel beam line (Figure 3.2). This will allow the measurement, with a picoammeter, of the current produced by the ion beam striking the slits.

3.2 I. Ion Acceleration and Mass Separation Section

Vacuum was maintained in the first beam line section by a single diffusion pump. The diffusion pump was placed between the accelerator and a gate valve. The rotary pump backing this pump was shared with four diffusion pumps in continuous operation on another accelerator system. The gate valve could be used to isolate the beam line from the accelerator so the beam line was not exposed to air when maintenance of the ion source was required. A second gate valve was included to divide the first beam line section from the differential pumping chamber.

Vacuum seals in this section were made using a conventional ~~O-ring~~ system. An ionization gauge was used to measure pressure.

3.3 Beam Line Sections II and III: The UHV Apparatus

The target chamber residual pressure is expected to be less than 10^{-10} torr, although this will rise when the ion beam is introduced. To achieve this pressure, both the target chamber and the differential pumping chamber were of bakeable stainless steel construction. Most of the seals consisted of a copper gasket compressed between two stainless steel flanges. The flanges were evenly tightened together with bolts, equally spaced around the flanges' perimeter. Raised knife edges on the flanges' sealing surfaces bit into each gasket, deforming the copper to fill available gaps. Most gaskets were tightened only enough to prevent vacuum leaks, so they could be reused two or three times in the future (see Section 3.4).

The sample chamber was a standard 305mm diameter cylinder, 508 mm high, with multiple ports. Two of the ports were pyrex windows of 150mm and 100mm diameter. At the time of vacuum testing, the sample chamber was equipped with a nude ionization gauge and a titanium sublimation pump (TI pump). Pumping was accomplished via a diffusion pump and liquid nitrogen cold trap combination, of 600 l/s pumping speed. The TI pump will be reserved to achieve the best possible vacuum prior to starting each experiment. Also to be included, in the sample chamber, was the sample manipulator/goniometer and the rotating platform for mounting the detectors (Figure 3.3; Section 3.5).

The entrance port was connected to the differential pumping section via a straight-through all-metal valve in line with a flexible bellows, of

38mm inner diameter. The second 0.5mm slit will be mounted on a "zero length" double-sided flange, inserted between the entrance port and the all-metal valve. A modification to this flange has been investigated to accommodate a 25mm diameter pipe extending 75mm into the sample chamber, for the mounting of anti-scattering slits.

The large volume of the differential chamber was defined by a long straight flanged pipe and four-way cross, both of 150mm inside diameter, for a combined length of 733mm. This section was pumped by its own diffusion pump/ cold trap combination (pumping speed 300 l/s), attached to one side of the 4-way cross, with a second ionization gauge mounted directly opposite. At the downstream end, an adjustable support made horizontal and vertical alignment movements possible, using two separate turning screws of 1/2 inch and 1/4 inch diameter. At the upstream end it was supported by the cold trap, mounted on a movable platform, with tapped holes for four vertical 1/2 inch screws in the corners for height adjustment. In this way the first 0.5mm slit, marking the entrance to the differential pumping chamber, can be adjusted relative to the second 0.5mm slit.

Both diffusion pumps for the UHV apparatus were backed by the same mechanical roughing pump. The roughing system was designed to allow the differential pumping chamber and the sample chamber to be pumped down independently. A right-angle all-metal valve connected the sample chamber directly to the backing line, to ease initial pumpdown. In line with the all-metal valve, an up-to-air valve was included. Each pumping route: 1. from the large diffusion pump, 2. from the small diffusion pump, and 3.

directly from the target chamber, could be isolated from the other two routes via three in-line butyl valves. Thermocouple gauges were used to monitor the pressure in these sections. A bakeable foreline trap, filled with a molecular sieve material, was located next to the mechanical pump. Four flexible bellows were included: three to separate each of the three pumping routes from the UHV apparatus, a fourth was included to isolate the vibrations produced by the mechanical pump from the roughing system (Figure 3.4).

3.4 Vacuum Production

3.4.1 Laboratory Preparation

A few cautious laboratory preparations for the UHV apparatus were made, so as to ensure a long-life trouble-free operation of the UHV system. A clean room environment also facilitates sample handling and preparation. Exposed concrete in the vicinity of stored UHV components and the UHV apparatus was either painted or covered over, to reduce the hazard to UHV sealing surfaces by concrete dust. This included the concrete blocks used to raise the beam line and the UHV apparatus. Sealing raw concrete was recommended by other workers with UHV equipment (30).

In addition, most UHV systems backed by a roughing pump either vent the pump exhaust outside or employ an oil mist filter. Simple oil mist traps were installed on those roughing pumps in the laboratory, which did not already have a suitable trap. These traps were designed to use standard automobile air filters. Although not the best solution, they were an improvement to no oil filters at all.

As well, polyethylene gloves and bags were used to handle and protect flange sealing surfaces from skin oils and dust, etc. Isopropyl alcohol was used to clean tools coming into contact with UHV components, e.g. tweezers, feeler gauge, etc. The zinc coated (galvanized) storage shelves were also painted.

3.4.2 Roughing Line

There were problems with worn spring retaining rings, which did not stay fitted upon opening and closing the in-line valves. New retaining rings were unavailable; this type of in-line valve is no longer manufactured. Supports along the roughing line were included to keep the roughing line stationary while turning the valves.

A satisfactory backing line vacuum < 10^{-2} torr was achieved after an extensive initial bake of the molecular sieve material.

A vacuum test rig was used to calibrate the thermocouple gauge heads.

3.4.3 Differential Pumping Section

For vacuum testing, the beam line entrance flange on the 4-way cross was blanked off. On the UHV chamber side, the 70mm bellows was blanked off. Leak testing was performed employing a helium leak detector, sensitive to 10^{-10} std cc/s (1 std. cc/s = 0.76 torr-litre/s). No leaks were detected in the UHV apparatus at 3 X 10^{-7} torr, soon after the diffusion pump was turned on. Pumping over a few days achieved a pressure of 9.5 X 10^{-9} torr, after gauge degas. After baking overnight at 205°C, liquid nitrogen was added to the cold trap. The temperature was measured with a thermocouple wire attached to a flange bolt. The vacuum improved to 7.4 X 10^{-10} torr.

3.4.4 UHV Chamber

The start-up vacuum procedure was as follows:

1) The rotary pump was turned on to rough the system.

2) The poppet valve to the diffusion pump was slowly cracked open. The system was checked for leaks at 10^{-7} torr. As with the differential pumping chamber, no leaks were found.

3) The chamber was baked with the diffusion pump on. The pyrex windows were covered with aluminum foil to prevent heat stress.

4) The chamber was cooled to below 90°C and the oven dissassembled.

At this stage, the pressure had not improved past 10^{-7} torr. A leak had escaped detection. If the baking step had been successful, then

5) LN_2 would have been inserted into the cold trap, to pump the water out of the system.

Further leak testing led to the discovery of the lack of a copper sealing pad in the right-angle all-metal valve. The leak had been from the UHV chamber to the roughing line, not to the outside, and hence had not been initially detected. Spare sealing pads were then procured.

3.4.5 Accelerator and Beam Line

The first beam line section was also helium leak tested after initial assembly and pump down. Leaks were found along the O-ring seals covering the unused exit ports of the 30° magnet. The scratched metal plates pressing against the O-rings were replaced with new, unscratched ones.

The diffusion pump oil was checked for traces of iodine, from previous use. As well, the ionization gauge head was replaced with an uncontaminated one. The least pressure then measured was 2 X 10^{-7} torr after repeated degassings of the ionization gauge (5 X 10^{-5} torr prior to degassing).

3.5 Scattering Geometry

3.5.1 Sample Position

The sample is to be located 189mm downstream from the second slit and 60mm downstream from the antiscattering slits. The intensity in the beam is enough so that both collimating/vacuum-dividing slits can easily be 0.5mm, rather than 1mm as originally permitted, reducing the beam to one quarter of its power. This is important for grazing incidence, in order to keep the beam's area on the target surface to a minimum. One could choose the slit size depending on the incident angle of the beam. The antiscattering slits must be placed at least beyond the swept radius of the sample holder, 30mm. Wires to the sample holder must also be avoided, increasing this limit somewhat.

The sample will be located at the centre of the scattering chamber, at the focus of the upper chamber ports, mounted on an xyz manipulator / $\theta\phi$ goniometer (Vacuum Generators HPT series), with electron beam heating up to 1200°C. The sample can be exchanged through the top port by removal of the goniometer, or through the 150mm side port. Electron beam heating will be performed with an available power supply. As well, sample cleaning experience has been obtained via the use of electron beam heating (see Section 5.0).

The sample holder's degrees of freedom will allow the crystallographic directions of the single crytal target to be specifically aligned or randomly aligned with the incoming beam, in addition to choosing the incident beam angle.

3.5.2 Rotating Platform

A rotating platform and its support were designed, machined and assembled, on which to mount detectors, i.e. channeltrons arranged to perform charge fraction measurements. The rotating platform was designed to align the detector system with the specular reflection angle and other angles. The platform could be rotated up to 120° in the horizontal plane. A rotating bellows arrangement was added to allow manipulation of the platform location from the outside, limiting the range to the larger angles with respect to the incoming beam. A scale in degrees was marked on the platform edge to visually align the platform through the larger of the two viewing windows. When aligning the beam, any detectors mounted on the rotating platform can be safely rotated away from the beam's path.

The rotating platform itself consisted of a stainless steel pie-shaped wedge, of 50° of arc. It rested on 3/8 in. stainless steel ball bearings along its arc, and on a single ball bearing at the centre of rotation, coincident with the centre of the target chamber. The ball bearings were kept separate by a thin curved plate with equally spaced holes, and rested on a support structure consisting of a number of assembled pieces (Figure 3.5). The pieces were of thick construction so as to be reliable for reproducible measurements: the platform would tend to settle the maximum amount each time, as well, the warping of the pieces during baking would be minimal. In the event of necessity, the platform and the support can be disassembled for removal through the 153mm diameter

upper ports.

The platform was prepared for placement in the UHV chamber as follows. The platform pieces were commercially electropolished (by a company that electropolishes for a local UHV equipment manufacturer). The pieces were then rinsed in an ultrasonic bath and then with deionized water. The electrocleaning removed the machine shop grease and also showed where steel, rather than stainless steel, had been accidentally included. Tapped holes were also excellently cleaned in this manner. Electrocleaning has been used by Holmen et al. (2). Details concerning electrocleaning for different metals are given by A. Roth (31).

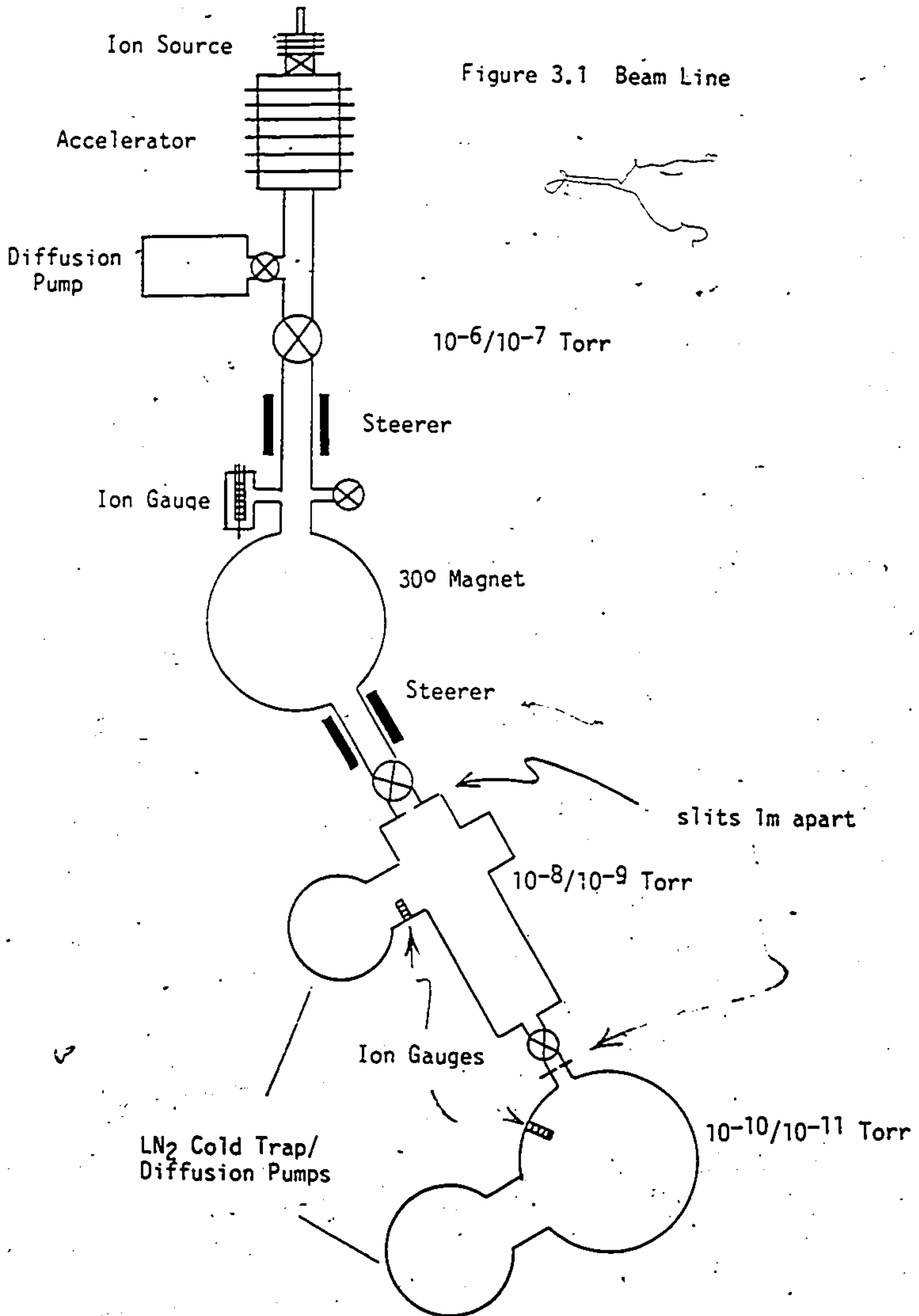

Figure 3.1 Beam Line

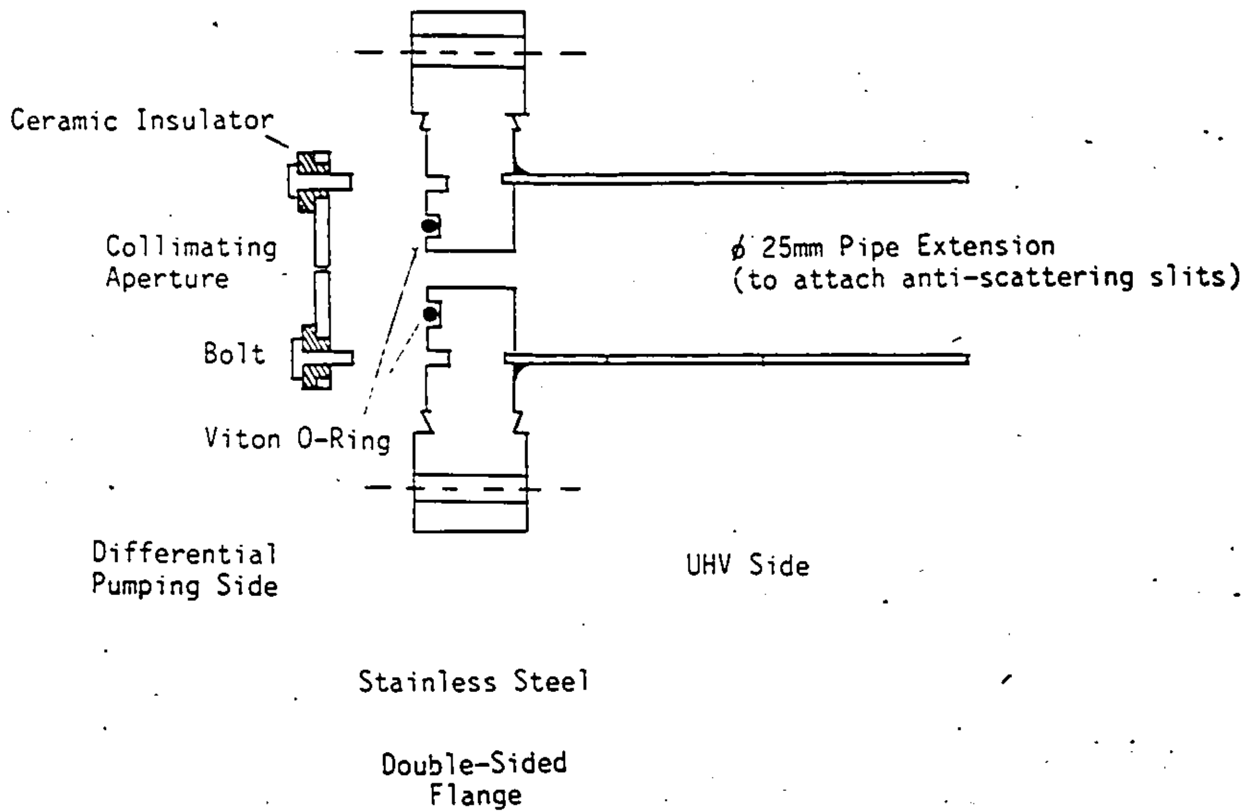

Figure 3.2 Second 0.5mm Slit
(Approximately to scale)

Figure 3.3 Target Chamber

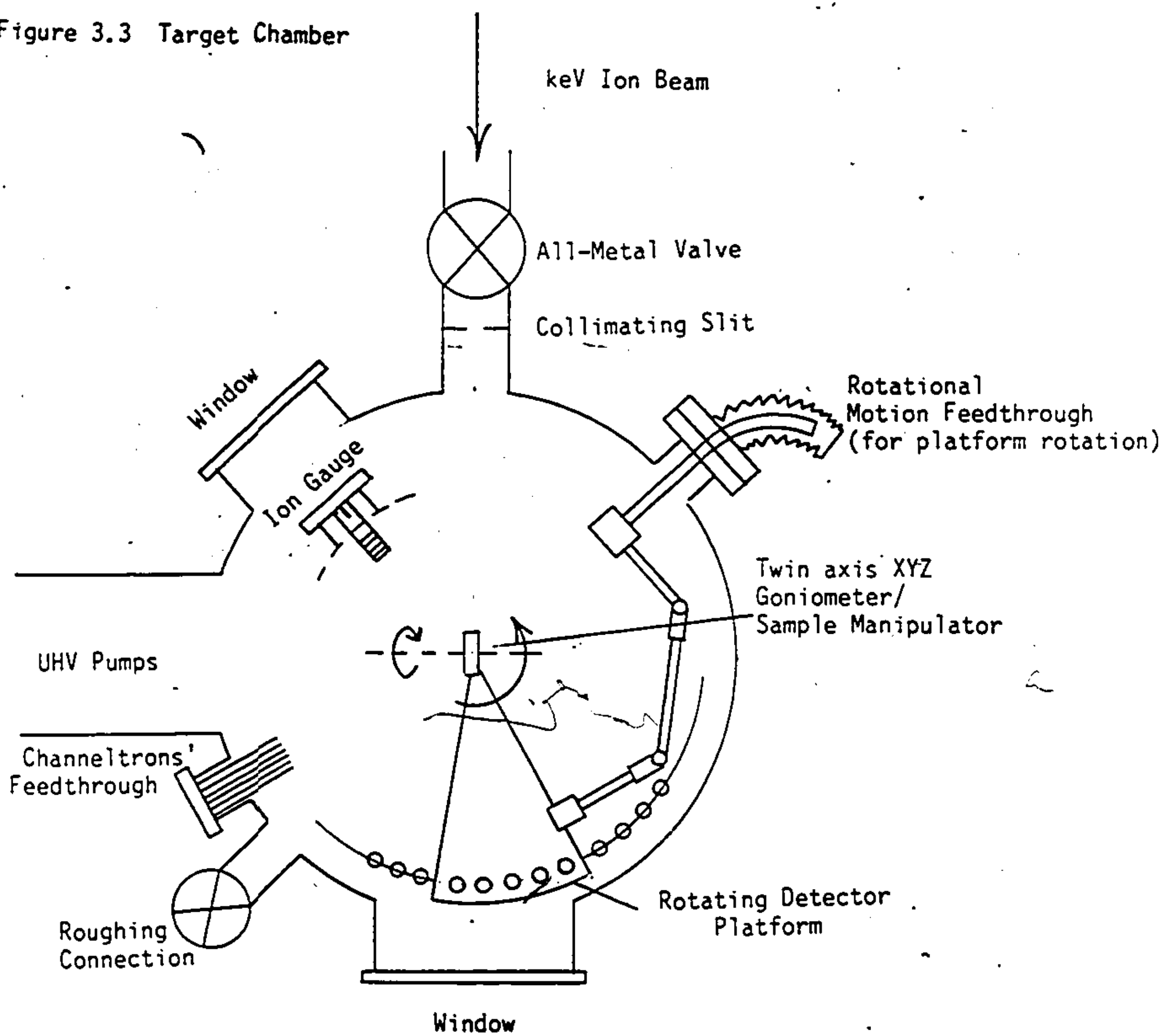

Figure 3.4 Schematic of Roughing System

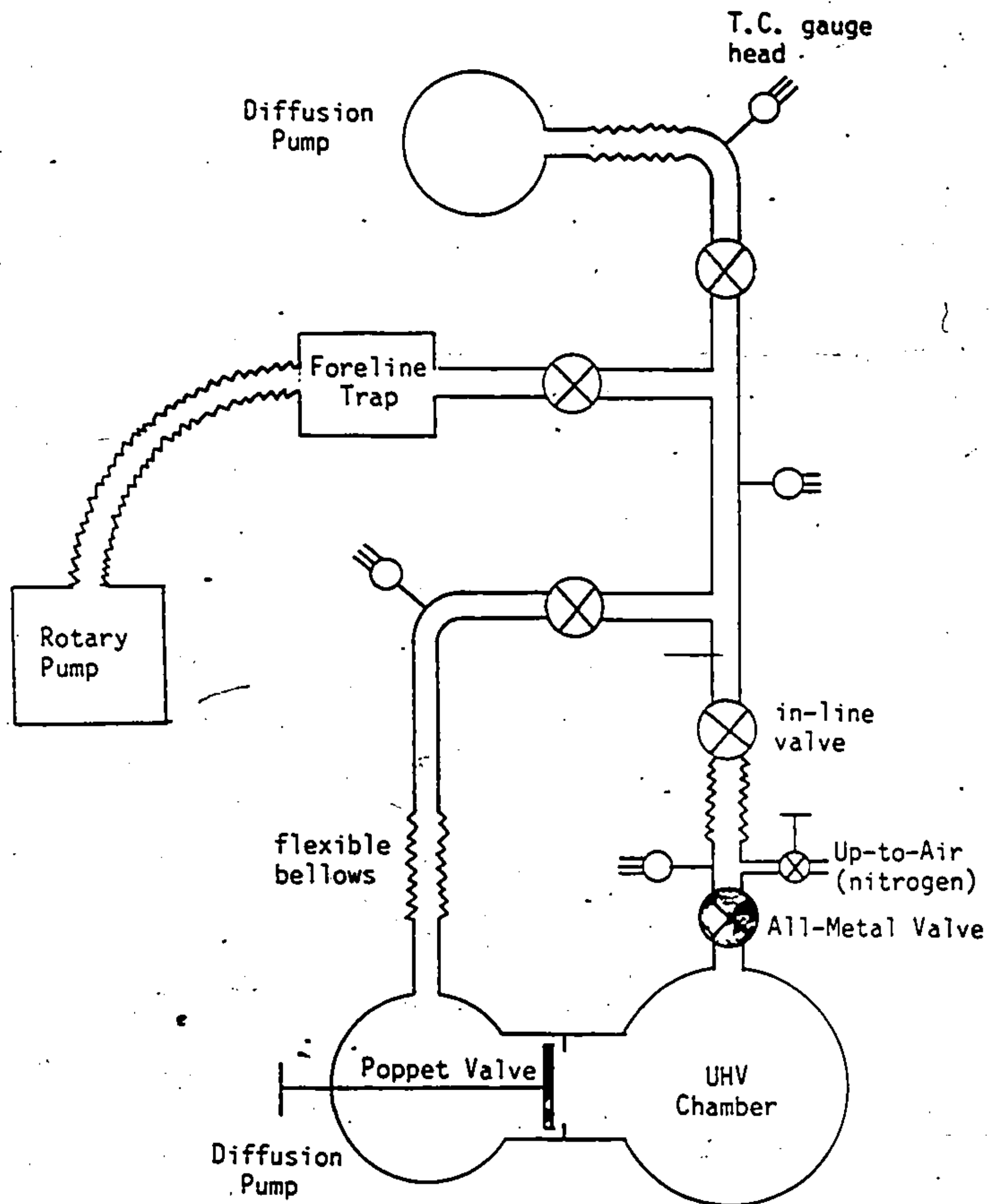

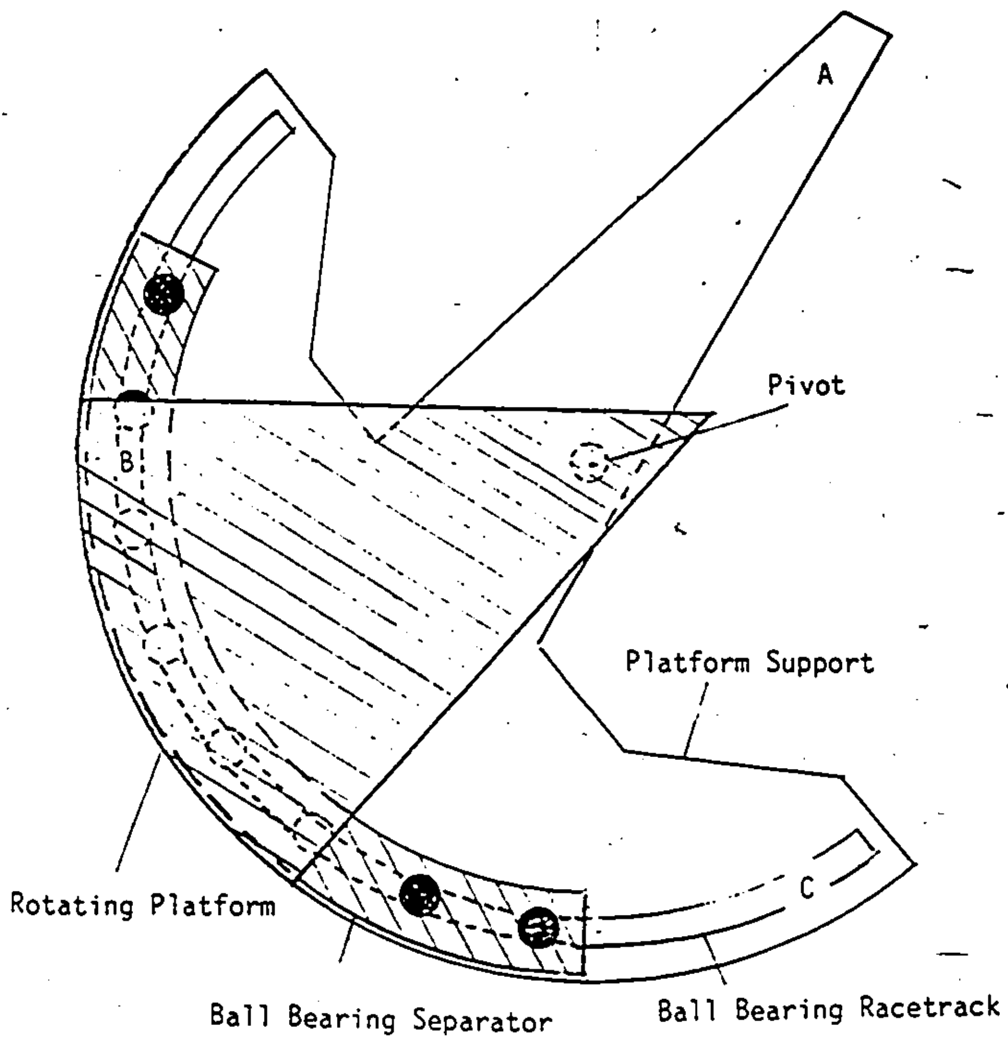

The platform support rests on a tripod structure topped by 3 ball bearings at A, B and C.

Figure 3.5 The Rotating Platform

4.0 Bakeout Oven

4.1 Introduction

Baking, in order to remove contaminants, is a necessary part of the UHV achievement process. The various commercial materials used in UHV are bakeable to 200°C, have a low outgassing rate and, when forming part of the vacuum envelope, negligible gas permeability (32).

Standard UHV hardware is mostly built of stainless steel (often Type 304) and can be baked at 450°C. Stainless steel remains relatively inert during exposure to the atmosphere at temperatures up to 500°C (3). However, vacuum components such as valves, demountable seals, and electrical and mechanical feedthroughs are often commercially made of materials that are only safely baked at lower temperatures.

The present apparatus includes Viton O-rings in the main shut-off valves to the cold traps, requiring a maximum baking temperature not more than 250°C (with the valves open). As well, the right angle configuration jack sockets, of the electrical feedthroughs in the manipulator flange, are specified by the manufacturer to be baked to only 200°C. At AECL in Chalk River, 135°C was considered a critical temperature where the majority of the oxygen and hydrogen absorbed into the stainless steel was released and could be pumped away, to reduce outgassing rates. The AECL group's chamber, after baking to 150°C, achieved pressures in the 10^{-11} torr range (15). Hence 200°C was reasonably chosen as the targetted upper limit for oven design.

The UHV apparatus uses materials with different thermal properties, e.g. the rates of expansion and conduction, and heat capacity. The rate at which the assembly is heated and cooled is critical. For stainless steel, rates of heating up to 2.5 degrees per minute are acceptable. Problems, with a faster temperature increase, include uneven heating which produces stresses on flanges and seals. Pyrex windows are especially susceptible to this uneven baking. A bakeout oven must have the capability of controlling the rate of temperature change.

4.2 Support Table and Oven Design

A supporting table was required on which to mount the UHV apparatus, both the sample chamber section and the differential pumping section. Table dimensions were chosen to fit the desired configuration of the equipment. Table height was chosen originally to match the accelerator beam height of 122 cm. However, the large diffusion pump would then hang lower than the expected table height would allow; the feasibility of putting a hole into the laboratory floor was examined. The other alternative was to raise the beam line and the UHV equipment up on blocks; this solution was eventually chosen as the most convenient one.

The table was designed as a two-height, or split-level, table (Figure 4.1). The sample chamber and its cold trap/diffusion pump combination were to be mounted immovably on the lower height table section. The differential pumping section including its cold trap and diffusion pump were mounted on movable supports on the upper height table section. Everything mounted on the table top was to be enclosed by the bakeout oven, able to be easily assembled and disassembled. Diffusion pumps obviously cannot be baked; they were to be mounted beneath the cold traps through openings in the table top.

The table frame was constructed of two-inch angle iron for mechanical strength. The entire table top, including the vertical section dividing upper and lower table sections, was insulated with 1 inch thick Fiberfrax Duraboard LD, a type of insulation able to withstand high temperatures and has good rigidity and stiffness. The insulation was clad in aluminum

sheeting to prevent its fibres, similar in messiness to asbestos, from escaping.

The bakeout oven's walls were designed to be stood up along the table top's edges (Figure 4.2). A 1 inch width of angle iron around the table's perimeter was left uncovered by the insulation. The oven walls were constructed of 1 inch thick Fiberglas Intermediate Service Board, able to withstand temperatures up to 450°C. This insulation was preferred over the Fiberfrax, because it was lighter in weight, easier to cut into shape, and inexpensive. It was rated with a thermal conductivity of 0.061 W/m°C at 250°C, slightly better than the Fiberfrax with a conductivity rating of 0.087 W/m°C. Aluminum sheeting surrounding the insulation gave structural support.

The finished oven consisted of an assembly of interlocking panels which mounted on the table top perimeter. Latches held the assembly together. Two additional panels could be placed to divide the upper and lower table sections, into an "upper oven" and a "lower oven". Each oven section could be assembled independently; each had its separate roof panel, which could be slid into place after the wall panels had been installed. Thus the baking of each section could be done either separately or together. In addition, the oven was easily assembled and disassembled by a single individual.

4.3 Oven Heaters

It was decided to use conventional oven 3000W heating elements as the heat source for the bakeout oven. This type of heating element was easily available. Its flat shape allowed vertical mounting on the oven wall panels, and would hence be removed with oven disassembly. The laboratory power required minimal modification to meet the circuit supply criteria of 220 Volts and 30 amperes. Lower voltages would have required extensive alteration of existing laboratory power: 115V, 750W heaters, for example, would have required 8 times as many extension cords. Higher voltages were not investigated.

A simple calculation to estimate heat loss through the oven walls was performed:

$$\frac{\text{Thermal Conductivity}(W/m^{o}C) \times 200^{o}C \times \text{Area}(m^{2})}{\text{Thickness}(m)}$$

This estimation was 4900W for the upper and lower ovens combined. The parameters used are those in Section 4.2 and Figure 2. Two 3000W heating elements per oven would hence provide sufficient heat for baking.

Since high temperatures would be encountered by oven wiring, high temperature wiring and ceramic terminal blocks were used. Number 12 wire was used throughout ($200^{o}C$ and $125^{o}C$ rating) for the 220V, 15A circuit. The $200^{o}C$ rated wire was used in the oven's interior. Its insulation is stable to $200^{o}C$ under continuous use; although it can be used above $200^{o}C$, it must be monitored for deterioration. The $125^{o}C$ rated wire was enclosed in BX for use outside the oven.

In the lower oven, the two heating elements were connected in parallel, originally to a simple "on-off" oven temperature controller. The controller allowed the oven's maximum temperature to be set ±10°C. During the "on" cycle, the controller applied full power. When the set point was reached, the power was switched off, although the temperature would increase a further ~10°C. The "off" cycle would then allow the temperature to drop to the set point before full power was again applied. The temperature would continue to drop until the heating elements had warmed. The initial "on" cycle caused too rapid heating of the system. The heating rate could only be slowed by utilizing many temperature settings in succession, separated by small increments, to achieve the desired temperature.

A new solution was required. The heating rate could be slowed by limiting the power to the elements. Limiting power to the system by connecting the two elements in series (750W maximum), successfully slowed the rate, but lowered the maximum temperature reached to well below 200°C.

An adjustable power control system was the next step. An inexpensive solution employing a triac (40 amp rating) was implemented, instead of an expensive Variac (6.6 kVA rating). A 3 inch wide ribbed aluminum heat sink of 6 inches in length was attached to the triac, determined from the method of (33), where the maximum power dissipation of the triac was chosen as 65W. A diagram of the triac controller circuit is given in Figure 4.3.

A diac was employed as a bilateral trigger to supply current to the triac gate. The potentiometer setting controlled the amount of time per half cycle the triac was on. A lamp was connected to the input side of the circuit so as to be on whenever the oven was on.

The triac required a choke for stable triggering. (Without a choke, the triggering of the controller would be uncontrollable.) One can design inductors using the approximate relation

$$L = \frac{\mu A N^2}{l}$$

where l is its length, A its cross-sectional area, N the number of turns, μ the permeability of the ferrite core, usually around 10^3 H/m. A piece of 3 inch ferrite of unspecified permeability, when wrapped 42 turns with #14 varnished wire, provided an inductance near 70 μH (as measured with an inductance bridge). This was near enough to the triac manufacturer's specification for a 100 μH RF suppressor choke.

4.4 Test Baking

4.4.1 Lower Oven Calibration

Once the wiring on the oven was completed, it was possible to test the heating circuit before the UHV apparatus had been shipped to the University. Although rates of heating were expected to be faster with an empty oven, it was hoped an equilibrium temperature could be calibrated for each potentiometer setting. The oven tested consisted of the "lower" oven, using the divider panels between the upper and lower table sections to form one of the four outside walls. The two heaters were connected in parallel on the same controller. Although the hole reserved for the beam line in the divider panels was covered over, the hole in the table top reserved for the large diffusion pump was not.

The first time the oven was turned fully on, 215°C was reached in ten minutes. The oven roof showed some warping. After half an hour with no power, the temperature dropped to 53°C. Intermediate potentiometer settings were therefore required during both heating and cooling to limit the rate of change to the maximum allowable 150°C/h. As well, 1/32" thick aluminum sheets, 50cm X 48cm and 42cm X 58cm, were installed to cover the two heating elements, so as to encourage convection air circulation and so give a more even thermal distribution. At this point the triac circuit was included (see Section 4.3 Oven Heaters).

To find the potentiometer settings corresponding to the percentage of total power available, currents were measured with the aid of an AC current clamp and mutimeter. The maximum current measured, at 100% power,

was 22.7A $\pm$ 0.2A $_{rms}$. The potentiometer dial was marked at fractions of the total power available. Due to the hysteresis in the triac circuit, the potentiometer dial was turned to maximum each time before returning to the chosen setting.

A compilation of triac circuit testing and calibration is given in Figure 4.4. Each curve represents where a different power was applied to the oven. The temperature was recorded as a function of the time elapsed since the oven had been turned on. Each test was commenced once the oven had returned to near room temperature.

An equilibrium temperature was extrapolated from each curve in Figure 4.4. The shape of the curves suggested that the temperature increase might be simply modelled using Newton's law of cooling, such that

$$\Delta T = \Delta T_o (1 - e^{-t/\tau})$$

where ΔT was the temperature difference between the heating elements and the oven's interior, and ΔT_o the temperature difference at time t = 0. From the graph, the time constants τ were estimated between 30 and 40 minutes.

4.4.2 Baking Procedure

Once the UHV equipment was assembled and the pumping system made operational, baking was performed as part of vacuum testing (see Section 3.4).

A record of the first two bakeouts of the differential chamber in the "upper" oven was plotted in Figures 4.5 and 4.6. In both instances the oven was cautiously, i.e. slowly, brought up to temperature. An

iron-constantin thermocouple, attached to a flange bolt on the apparatus, was used to measure the temperature of the stainless steel. A thermocouple thermometer was used to measure the oven air temperature in the vicinity of the flange bolt. It was endeavored to keep the flange-air temperature difference under control, since the temperature distribution in the oven was unknown.

The first bake was used to check for any difficulties in the operation of the oven. The oven was cooled via stops at 30%, 20% and 10%. On the second bake, the apparatus was left to bake overnight. The power was reduced once the flange temperature of 200°C was attained; equilibrium was attained at 40% power. The oven was cooled via stops at 30%, 10% and 1% potentiometer power settings.

A record of the first bakeout of the target chamber, enclosed by the "lower" oven, was plotted in Figure 4.7. The number of intermediate potentiometer settings was reduced from the number used with the upper oven.

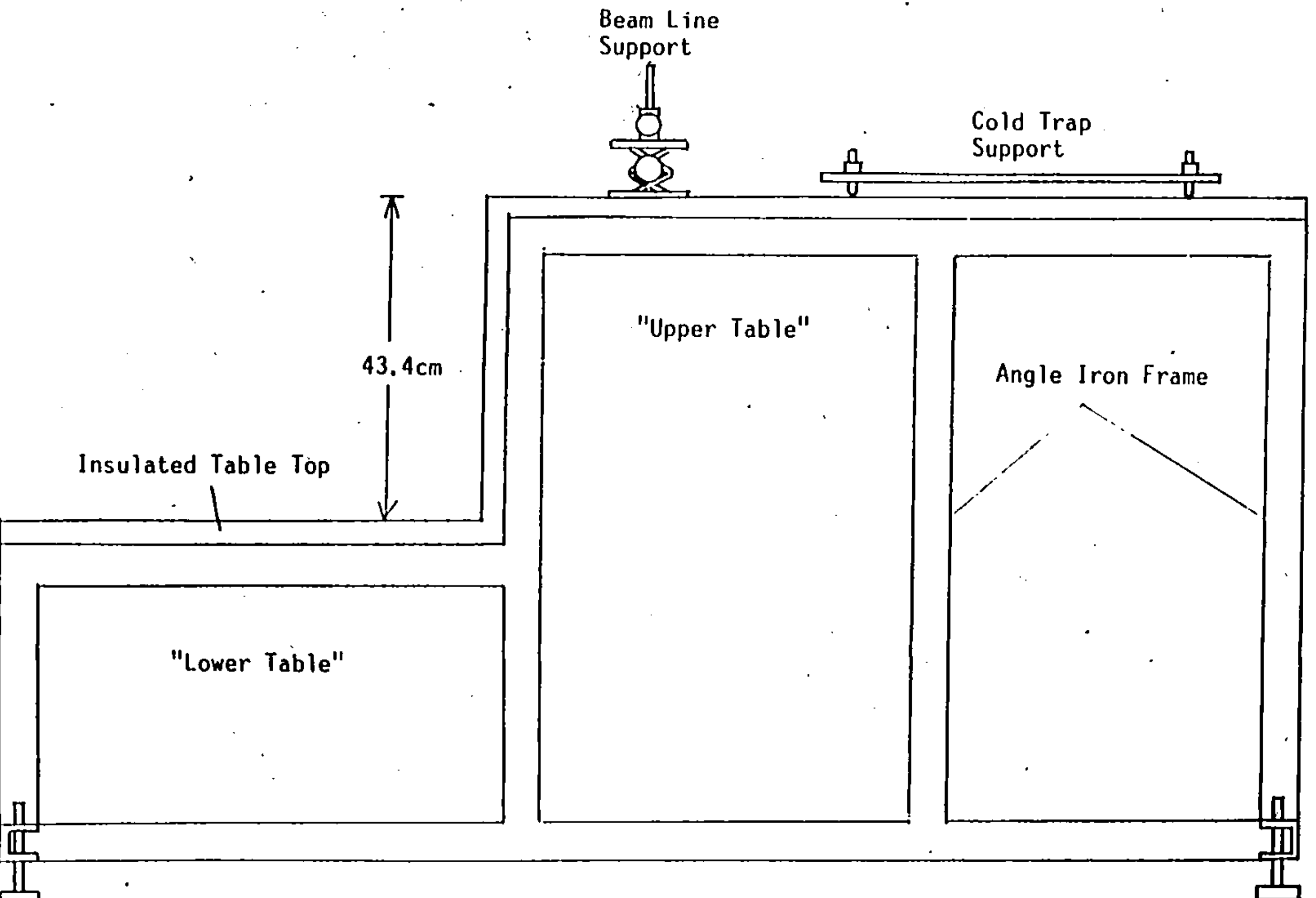

Figure 4.1 The Two-Height Table
(Side View)

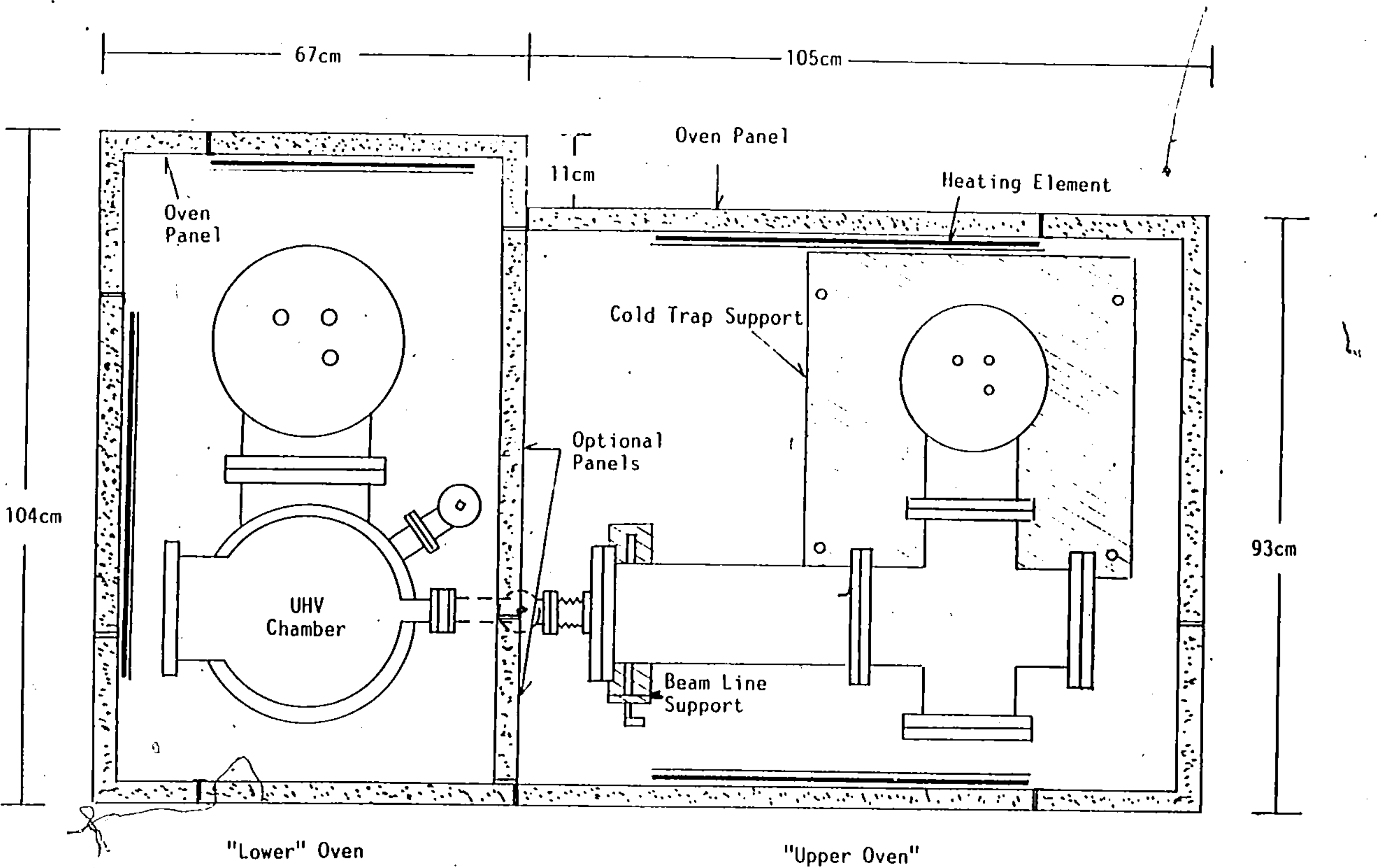

Figure 4.2 Top View of Bakeout Oven Showing UHV Apparatus

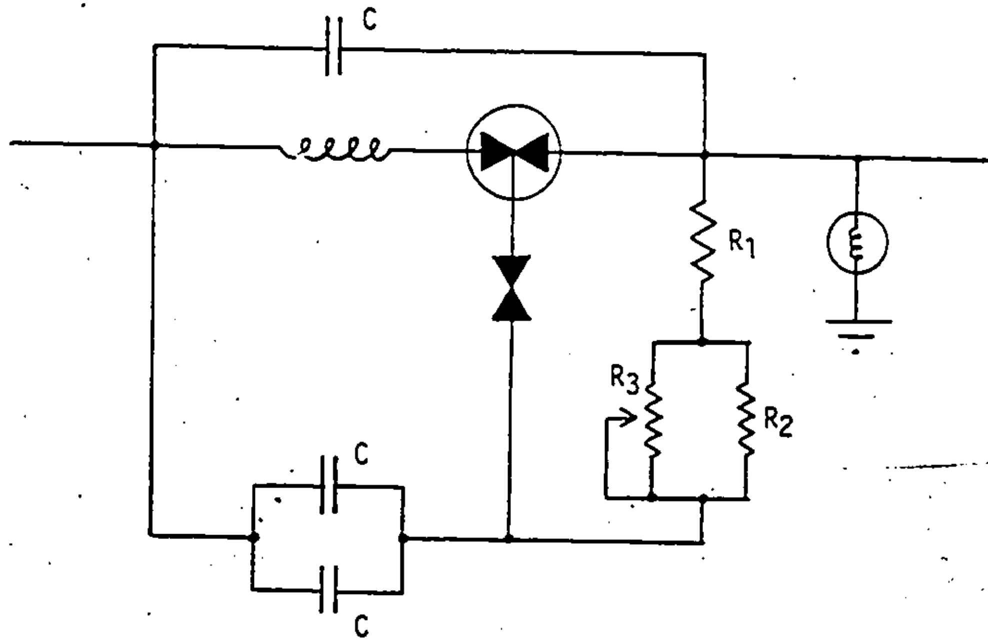

C = 0.1 MF
R_1 = 10 kΩ
R_2 = 560 kΩ
R_3 = 250 kΩ

Figure 4.3 The Controller Circuit

Figure 4.4 "Lower" Oven Calibration

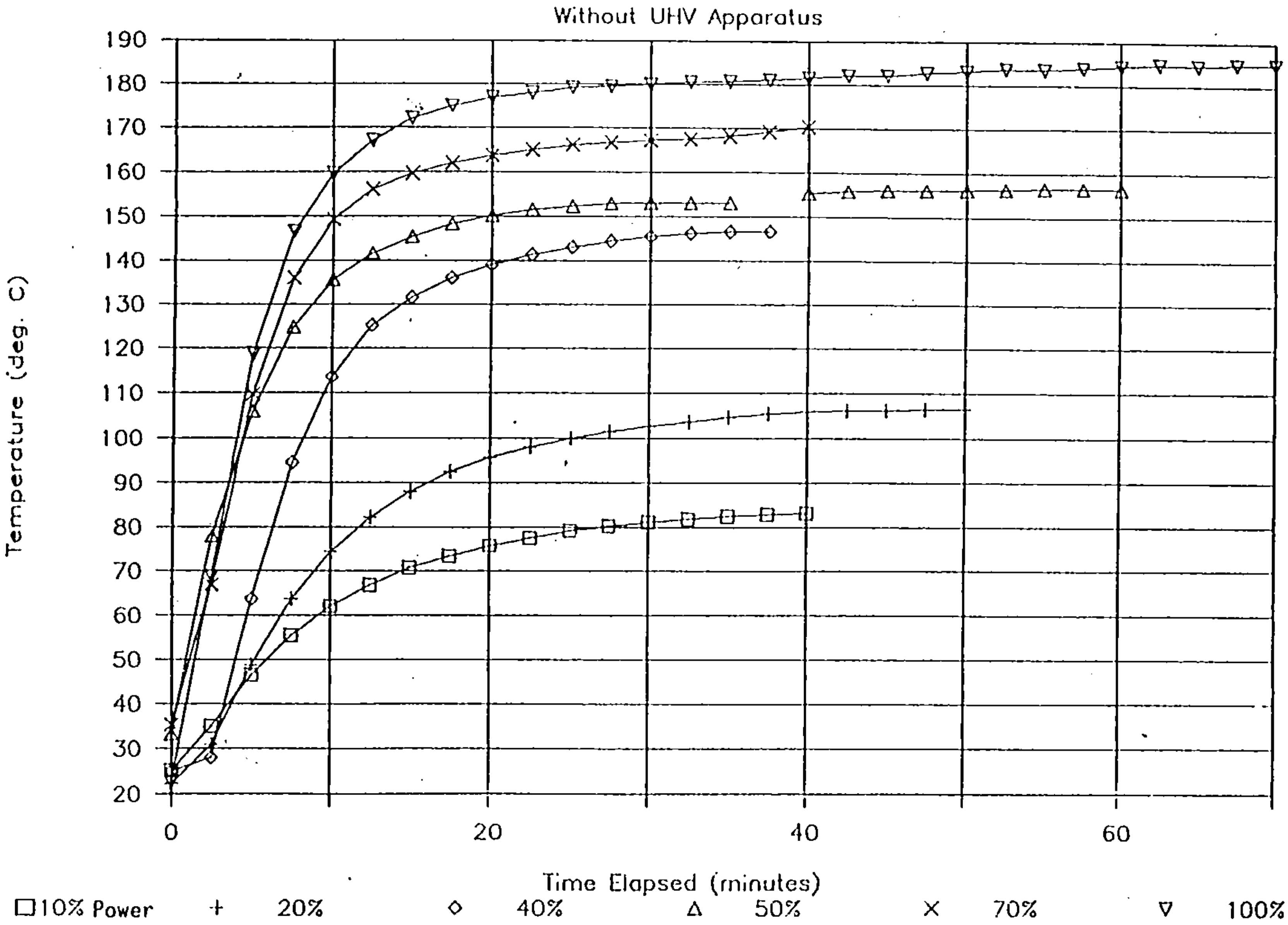

Figure 4.5 "Upper" Oven Bake

With Intermediate Chamber Apparatus

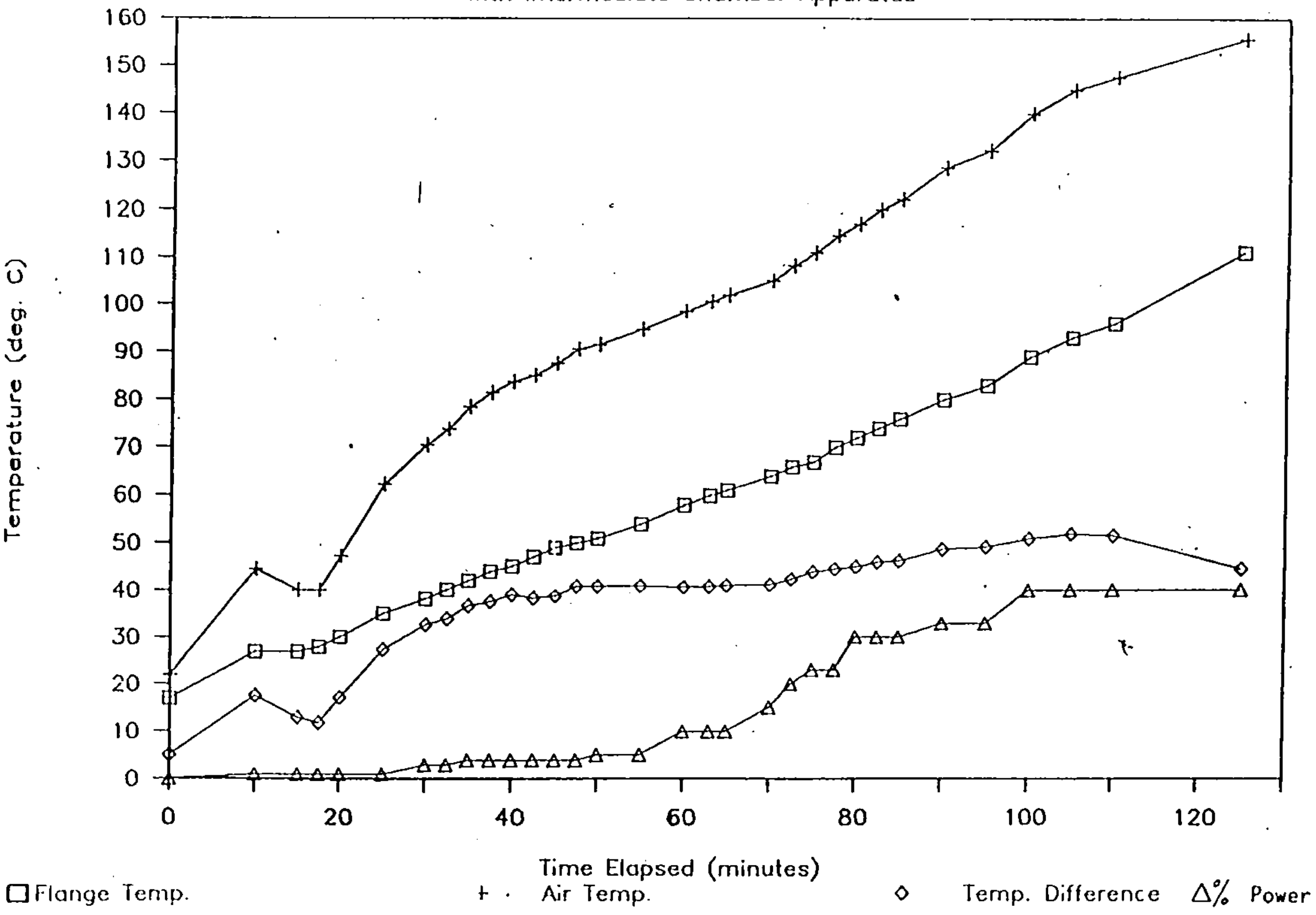

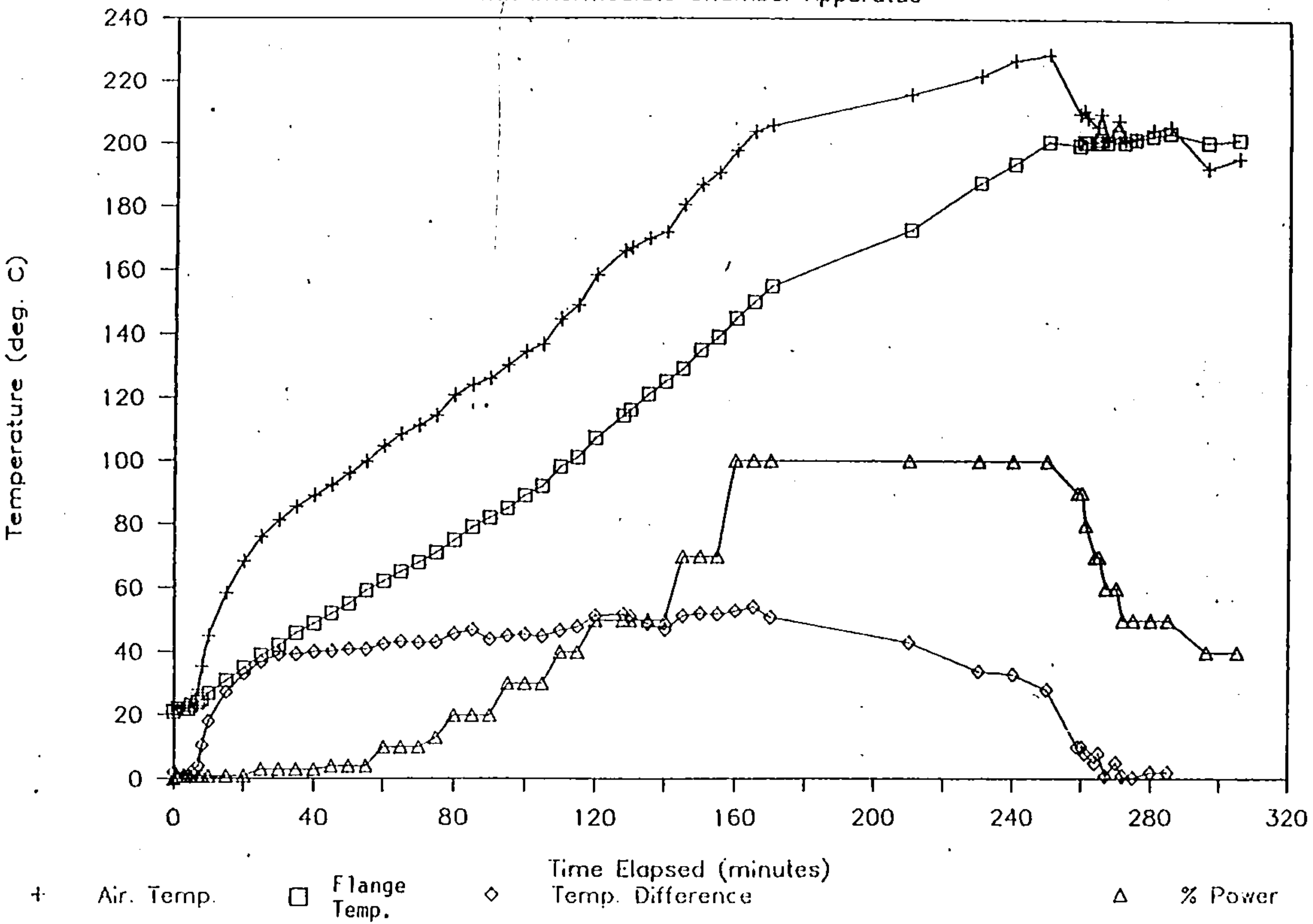

Figure 4.6 "Upper" Oven Bake #2
With Intermediate Chamber Apparatus
Temperature (deg. C)
240
220
200
180
160
140
120
100
80
60
40
20
0
0
40
80
120
160
200
240
280
320
Time Elapsed (minutes)
Air. Temp.
Flange Temp.
Temp. Difference
% Power

Figure 4.7 "Lower" Oven Bake

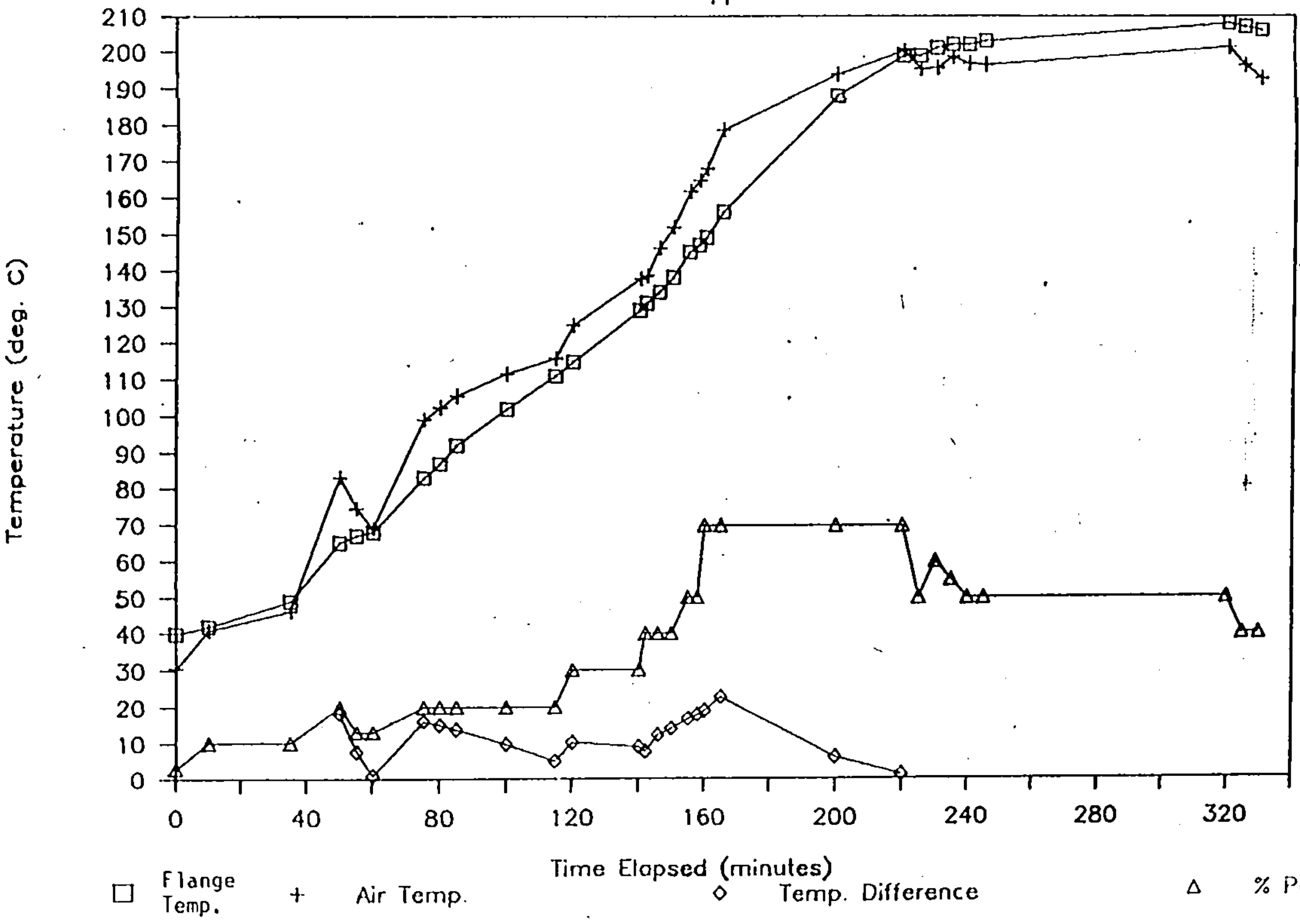

5.0 Si(100) Surface Preparation Measurements

5.1 Sample Preparation at NRC

In collaboration with Dr. Robert A. Armstrong at the National Research Council (NRC), the cleaning of Si(100) was undertaken. Clean silicon is considered fairly inert (compared to some metals) and hence believed to keep fairly clean after the removal of the oxide.

The cleaning of Si(100) has been the focus of many investigations, especially for achieving an atomically clean and defect-free surface for silicon MBE (Molecular Beam Epitaxy) (34-38). Clean Si(100) has also been a prerequisite for surface studies (10,39-43). The major contaminants of a manufactured wafer are carbon and oxygen. Annealing above 1200°C is often employed, as well as ion sputtering and annealing. At these temperatures residual carbon sticking to the substrate surface is removable. However, surface damage such as split lines and thermal pits has prompted investigations into methods effective at temperatures less than 1000°C (35,36,38) and as low as 710°C (37).

Low temperature cleaning in vacuum takes advantage of the reaction of the silicon substrate with the surface oxide, yielding volatile SiO. In UV ozone cleaning, the oxide is grown in an ozone reactor oven prior to loading the sample into the vacuum system. Until the sample is heated, the oxide acts as a protective coating, preventing further contamination (34,37).

At the National Research Council, samples of Si(100) were cut from a 4

inch wafer, treated with ozone, then the oxide removed in a UHV sample chamber equipped with both LEED (Low Energy Electron Diffraction) and AES (Auger Electron Spectroscopy) surface investigation apparatus. The proposal was to emulate the NRC cleaning procedure at the University of Ottawa.

5.1.1 University of Ottawa Requirements

The priority was to obtain a sample which could be easily cleaned in a UHV environment by following a standard procedure. One must have an atomically clean sample in the UHV chamber when measurements are ready to be taken. At present, the University's sample chamber is not equipped with surface analysis equipment such as LEED or AES. Hence the sample must be prepared without measuring its condition. In future, it is hoped a HEED (High Energy Electron Diffraction) system will be added.

5.2 Electron Methods for Surface Analysis

Two widely used surface analysis techniques are LEED (Low Energy Electron Diffraction) and AES (Auger Electron Spectroscopy). Both rely on information obtained from collisions of nearly monoenergetic and well-focused electrons with surface and near-surface atoms.

5.2.1 LEED

LEED provides information about the periodic two-dimensional lattice structure of the surface. Changes in a surface's diffraction pattern can result from the appearance of contaminants or from the reconstruction of a clean surface.

Many surface structures, such as Si(100), can be described using an abbreviated form of Wood's notation as an (n x m) structure, where n and m are the integer ratios of the surface mesh vector lengths to those of the bulk, such that the surface and bulk vectors are parallel. The letters p or c are often included to indicate if the surface structure is primitive or centred. Other surface structures, involving a rotation of the surface structure with respect to the substrate, are described using the complete form of Wood's notation. In addition, all surface structures, including complex ones, can be described using matrix notation (4,24,44).

5.2.1.1 LEED Experiment

The operation of the low energy electron diffraction system at NRC was as follows:

The sample, secured to a manipulator system, was situated to face the LEED electron gun and hemispherical mirror analyzer (Fig. 5.1). The sample's height was adjusted so the electron beam would strike the centre of the sample; the sample was rotated to optimize the clarity of the LEED image. The electron gun was of the electrostatic type, beam voltage 0 to 3000 V, beam current up to 1μA at 100 eV. The beam diameter was specified as <1mm at the specimen. The LEED pattern was produced by diffracted electrons striking the hemispherical analyzer. The analyzer consisted of hemispherical grids, each a chrome-plated stainless steel mesh (100 lines/inch), with a phosphor-coated stainless steel collector. Together the grids functioned to reject inelastic electrons. The collector was biased at a potential of plus several kV, to accelerate the electrons for the display. The diffraction pattern was viewed through a window into the sample chamber.

5.2.1.2 Interpretation of LEED Data

A LEED pattern of a chiefly periodic surface consists of an array of distinct spots and a diffuse background. The penetration depth at LEED energies is estimated less than 10Å; diffraction is limited to surface and near-surface atoms. The intensity in a pattern is affected by structural

disorder, roughness, precise crystallographic orientation, thermal diffuse scattering, etc (42,45). In general, a LEED pattern is not a sensitive indicator of the surface perfection. It only shows regularity on the scale of the surface region over which the primary electron wave field is effectively coherent, generally on the order of 100Å (coherence radius), although the cross-section of the electron beam is typically about $1mm^2$. Slip lines and thermal pits, for example, could not be detected (24,44,45).

5.2.2 Auger Electron Spectroscopy

Auger Electron Spectroscopy easily supplies information about surface chemical composition. AES can also be used for quantitative chemical analysis (39,46).

An Auger electron is an atomic electron receiving enough kinetic energy to be ejected, usually from the L-shell, when another electron falls from the same shell to fill a vacancy in the K-shell. Auger electrons are emitted when an energetic beam of electrons (1000eV - 5000eV) strikes the atoms of a material, causing the relaxation of initial core hole states. The Auger electrons will have energies appropriate to the atomic levels where they originated. Their emission is assumed to be isotropic. Hence energy analysis enables identification of the materials present (4,24,44). In this case, element identification was accomplished with the aid of published energy spectra, in The Handbook of Auger Electron Spectroscopy (47).

There are different types of electron energy analysis systems, of which the cylindrical mirror analyzer (CMA) is one. A CMA of the window filter type was used in the present apparatus. In this type, electrons possessing a specific kinetic energy are focused at the detector aperture from passing between two coaxial cylinders with appropriate potentials (Figure 5.2).

The AES instrumentation included the electron gun control, the Auger system control, the lockin amplifier and the electron multiplier supply. Output was to an X-Y plotter. The Auger system control was set to sweep

rates of 4eV/s and 6eV/s, so that a spectrum could be obtained every two or three minutes.

The data was displayed as the second derivative of intensity d^2I/dV^2, as a function of electron energy, eV. This isolated the Auger electron signal from other electron loss mechanisms taking place simultaneously (Figure 5.3). Peak sizes assisted in quantitative AES.

5.3 Experimental

Sample cleaning trials took place in a UHV chamber pumped by a sorption and ion pump system (VARIAN VacIon). The sample holder was affixed to the front of a cylindrically hollow molybdenum block, 0.7 X 0.6 X 1.0 inches. The block housed the electron bombarder used to heat the sample (Figure 5.4a). This entire block was mounted on a z and theta manipulator which was differentially pumped using a teflon gasket sealing system. The sample could be rotated 360° in either direction around the central axis, specifically, to face the LEED electron gun and hemispherical analyzer, a further 90° to face the AES electron gun, and another 90° to face the viewing window.

The electron bombarder consisted of a tungsten filament of 25 or 40 turns wired to a 5kV 50mA power supply and a floating filament power supply (Figure 5.5). Gold wires, chosen because of their flexibility, were spot welded to the electron bombarder. The electron bombarder was mounted in a vacuum fired alumina cylinder, insulating the filament and its surrounding shield from the molybdenum block and sample holder. The molybdenum block and sample holder had been originally vacuum fired at 10^{-6} Torr and 1000° C.

Temperature measurement was by optical pyrometers: a disappearing filament type and an infrared detector type. In the future the thermocouple on the sample heater at the University of Ottawa can be calibrated to these pyrometers. Background pressure and partial pressures were monitored with a residual gas analyzer equipped with a Faraday cup

and a scanning electron multiplier (SEM). Five samples were heated.

Changing samples was accomplished by lifting the manipulator, with sample holder, out of the vacuum chamber. The old specimen was removed and a new prepared specimen installed. The manipulator assembly was then replaced in the chamber, its flange bolted to the chamber flange for a new vacuum seal.

To change samples, the chamber was first brought up to atmospheric pressure by backfilling with Argon. After the manipulator was removed the opening was covered with a blank flange. This kept the system dry so the sample chamber did not require baking. This improved the rate at which new samples were introduced to UHV. Two or three days were allotted between initial pump down and sample heating trials to improve vacuum conditions. Details of the pumpdown and sample outgassing are reported in Section 5.4.

5.3.1 Ozonated Si(100) Wafer

The procedure used to prepare the silicon samples, prior to installation in the vacuum chamber, is described.

Pieces from a 4 inch diameter commercially manufactured silicon wafer (Wacker hyper pure) were cut to fit a molybdenum mounting plate. Cutting was initiated perpendicular to the flat (edge). For this wafer the flat was along the 110 direction. The method of cutting was as follows:

1. The wafer was placed on a few sheets of stacked onion skin paper for cushioning.
2. The location of the cut, perpendicular to the flat, was decided.
3. A jeweller's screwdriver was placed a few mm from the edge of the flat, along the proposed location of the cut. This kept the wafer from flying away while cutting.
4. The crystal was scratched with a diamond scribe: from the tip of the screwdriver, off the edge of the flat, at right angles to the flat. This split the wafer in two, in the direction the crystal was scratched.
5. The wafer was repeatedly cut into pieces, at right angles to the flat edges, until the desired size of crystal was obtained. Straighter cuts were achieved using wafer pieces of a square (rather than rectangular) shape. This was found to be true when obtaining a piece to fit the mounting plate, 0.5 in. X 0.3 in.

A sample was then positioned on the plate with tweezers. A length of tantalum or tungsten wire was used to secure the sample in place. The wire was wrapped around one molybdenum screw, crossed over the sample

face, wrapped around the second molybdenum screw, then crossed over the sample face again via the third and fourth screws (Figure 5.4b). The wire and the tweezers had been prepared for vacuum by cleaning in an ultrasonic bath: five minutes in acetone, followed by five minutes in isopropanol.

Next the sample and sample mount were baked in the ozone reactor oven for 3000 sec. This has been determined to be the most optimum setting for achieving a sufficient (workable) oxide on the surface, although the thickness of the oxide layer is not known. The sample was then ready for installation in the UHV chamber.

5.4 Sample Measurements

Power to the electron bombarder was increased in increments so that the power settings and corresponding sample temperatures were recorded. The infrared detector pyrometer was adjusted for a total emissivity, e, of 0.8, for silicon. The disappearing filament pyrometer had no emissivity adjustment; instead its temperature readings corresponded to the brightness temperature of the object. Ideally, the expected readings of the two pyrometers would be related by

$$W = e\,\sigma T^4 = \sigma T'^4 \qquad (48)$$

where W is the radiant emittance (watts/m^2) of a surface that is not ideally black, T its temperature and T' its brightness temperature. At many of the temperature settings, the sample was rotated 90° to face the Auger electron gun for an AES scan to monitor the condition of the surface. The power was reduced during scans.

Preliminary measurements were made with a Si(100) sample already in the UHV chamber, the only one of the samples not initially coated with oxide. The measurements on this sample and four ozone-treated samples are individually described in order as follows. Information with respect to the level of detection of impurities is collected in Table 5.1 (see Section 5.4.6 Summary of Sample Measurements).

5.4.1 Argon Bombarded Si(100) ("Zeroth" Sample)

This sample had both a molybdenum backing plate, to prevent electrons from bombarding the sample directly, and a molybdenum cover plate with a

circular opening of 0.25 inches, also made from molybdenum. This sample had been sitting in the UHV chamber for six months without cleaning, then was bombarded with positive Argon ions (sputtering).

AES showed the Argon had imbedded in the Silicon. There was also a large amount of Carbon present (47, Figure 5.6). LEED images of this sample showed fuzzy spots and a bright background.

The Auger also showed a peak whose position depended on the electron current of the detected electrons. This "spurious" peak was believed to be caused by electrons colliding with the detector aperture. The spurious peak was in the Auger part of the spectrum and not at high enough energy to be in any way associated with the electron elastic scattering peak. (Fig. 5.3). The primary beam energy was 2.5 keV , which was well above the Auger energies of interest (0-600eV). The spurious peak was moved from the region of interest by changing the focus, but could not be entirely removed. The sample face to the Auger electron gun opening distance was checked with a traveling microscope. This distance was 0.67 +/- 0.3 mm whereas the recommended location was 0.65 mm. Therefore a problem in focus resulting from the sample location was eliminated as the cause of the spurious peak. The spurious peak was also present for all subsequent samples.

After heating to 1060°C, measured with the disappearing filament pyrometer (1060°C D.F.), aimed to one side of the sample, no LEED pattern was visible. The best Auger trace showed Argon imbedded in Silicon. The ratio of carbon to silicon peak heights was 1:7. The next day LEED showed light spots up to a beam energy of 450 volts i.e. after the sample had cooled completely.

5.4.2 First Ozone Treated Sample (No. 1)

The method of fixing the silicon to the sample plate was modified. First, an unused sample plate and its four molybdenum screws were vacuum fired at 10^{-6} torr and 1000°C for many hours to outgas them thoroughly. Then tantalum wire, in place of the molybdenum cover plate, was used to secure the sample (Section 5.3.1). This was to expose more of the sample to surface analysis and to reduce its thermal contact with the sample holder. Also no backing plate was inserted. In this instance, tantalum wire was chosen because it was cleaner than the available tungsten wire. Tantalum is less brittle and it was easy to bend the wire around each of the four screws. There was a small concern that tantalum might diffuse into silicon while heating; silicon is known to be a solvent for various elements.

After the ozone treatment, the sample was delayed from immediate placement in the vacuum chamber. The shield surrounding the electron bombarder filament had come loose, and required spot welding to its connecting leads. The gold wires connected to the filament and shield needed to be removed for access; these wires had to be replaced and spot welded as well. It was five hours before the oxidized sample could be placed in the UHV chamber and pumping started. Overnight the total pressure reached $\sim 1 \times 10^{-9}$ torr; the H_2 peak was ten times greater than all other contaminant peaks.

Prior to performing sample measurements, the electron bombarder filament, and the LEED and Auger electron guns were turned on for an hour

to outgas them. With the getter pump used afterward, the pressure improved to 1 X 10^{-10} torr. It was decided not to bake.

Before heating, AES showed the presence of SiO_2, C and O. The SiO_2 peak shape resembled that of bulk-like SiO_2, as opposed to thin-layer SiO_2 or the intermediate oxide (46, Figure 5.7) In this case only the infrared (I.R.) pyrometer was used to measure sample temperature.

With the electron bombarder potential fixed at 1500 volts, the filament current was increased to 32 mA, at which time the recorded temperature was 810°C I.R. The current was reduced and an Auger spectrum obtained.

The sample was again heated at 1500 volts, 32 mA. This time the sample reached its melting point and a hole appeared in its centre. The melting point of Silicon is 1410°C. The current was reduced quickly; this created split lines on the Silicon face. However, all the oxide had been removed from the sample and a clear LEED image was obtained (bright, well-defined spots, dark background). A set of photographs were taken of the images at increasing beam energies.

Encouraged by the knowledge the silicon could be cleaned, this sample was removed from the vacuum chamber and another sample prepared.

5.4.3 Second Sample (No. 2)

On this occasion, the high voltage power supply proved to be faulty. It was replaced with a 1000 volt power supply and a standard analog milliammeter. Auger scans were taken at increasing temperatures. The pressure increased from the 10^{-9} torr range to 3 X 10^{-8} torr during this procedure. After heating to 1140°C D.F., there was still carbon on the sample and no distinguishable LEED pattern.

Molybdenum bending plates affixed to the manipulator axis had been used to support the sample holder/electron bombarder. The "benders" each consisted of two thin plates held together by a small amount of epoxy. The benders became suspect as a major cause of outgassing: they had been cleaned but not vacuum fired, and the entire sample holder had become hot during the sample heating.

5.4.4 Third Sample (No. 3)

A molybdenum backing plate was inserted between the crystal and the mounting plate. Electrons would strike the backing plate and the silicon would be heated by thermal contact with the plate. It was hoped more uniform heating of the sample would result. As well, the suspected benders were replaced by vacuum fired tantalum plates.

After initial pumpdown, mass spectrum peak heights showed a decrease of ~10 X overnight. The bombarder was next run at 5mA, 1000V. The

pressure rose to 3.2×10^{-9} torr, most probably due to outgassing hydrocarbon picked up during air exposure or deposit from the bender failure. The bombarder was run once more, overnight; afterwards the pressure was 1.4×10^{-9} torr.

AES showed the silicon was cleaned at 900°C D.F. (at 1000 V, 20mA; Figure 5.8). A distinct LEED image was obtained. While heating, the pressure was 2.6×10^{-9} torr. During surface analysis, the pressure returned to 1.5×10^{-10} torr.

Measurements were also taken across the sample face, to check on the uniformity of heating and cleaning. The face's centre was aligned to correspond to the Auger spectrum showing the most oxide removed. The sample "edge" was as far as the sample could be rotated without obtaining an Auger spectrum of the molybdenum frame. Relative carbon and oxygen Auger peak heights are presented in Figure 5.9, for data obtained ~1.5 hours after the "clean" Auger spectrum had been acquired. The peak shapes near 92eV were also compared against those for Si and SiO_2 presented in B. Carriere et al.(46). Crudely, the oxide monolayer was complete 1.7mm from the face centre and true SiO_2 appeared at 2.3mm.

5.4.5 Fourth Sample (No. 4)

The fourth sample was mounted with the backing plate present. It was outgassed at 800°C D.F. for two hours the day before heating, such that most of the oxide was removed, but carbon and oxygen peaks were still present. Prior to outgassing, the pressure was 2×10^{-9} Torr, afterwards it was 1.1×10^{-10} Torr. It was heated to 990°C D.F., from 900°C D.F. on one side to a hot spot at 1100°C D.F.

AES showed the sample was clean. The LEED image was the same as that for a clean p(2X1) surface (39). In this instance an area estimated nearly 4 mm in diameter had been cleaned.

5.4.6 Summary of Sample Cleaning Measurements

Information obtained from Auger spectra has been compiled in Table 5.1. Contaminants were generally restricted to carbon and oxygen, although Sample 3. showed the possible presence of boron. Boron may have been present during wafer manufacture or it may have been introduced from clean room tools while mounting the sample. The level of contaminants has been expressed as the ratio of the contaminant peak height (the peak-to-peak amplitude) to that of silicon. The background level, also expressed in ratio form, indicates the precision output by the A.E.S. system for each measurement.

Corrections were made for peak ratios where the contaminant peak had been measured at one focus and the silicon peak at another focus: changing the focus had been required in some instances as a method to evade the spurious peak. Corrections were also made for spectra recorded in two scales: the scale of a few Si peaks had been increased when the C and O peaks had become visibly small on a small scale. Errors introduced by these corrections are estimated less than or equal to the magnitude of the specific background ratio. The AES output signal was assumed isotropic and its resolution energy independent.

5.4.6.1 Temperature Measurement

Many temperatures were measured with both pyrometers. From these measurements, a correlation between the two pyrometers was obtained. This correlation is graphed in Figure 5.10. Temperature readings from the infrared pyrometer (°C I.R.) are plotted against brightness temperature readings from the disappearing filament pyrometer (°C D.F., "+" symbols). Disappearing filament temperatures corrected for 0.8 emissivity are also plotted (square symbols). However, they do not agree with the infrared pyrometer readings. Changes to the specimen's emissivity with removal of the oxide were considered negligible; silicon itself is nearly a black body.

The question arises what the actual temperatures were. All measurements were obtained to +/-10°C (D.F. or I.R.). The infrared pyrometer was initially aimed more to the sample edge, where it was cooler. Hence the corrected disappearing filament pyrometer readings are possibly nearer to actual values at the warmest part of the sample.

The electron bombarder power requirements for each sample are illustrated in Figure 5.11. Each sample shows a different heating curve of the measured brightness temperature as a function of power. This is mainly assumed to be caused by changes in thermal contact between each specimen and the specimen's mounting hardware and the sample holder. Samples No. 1 and No. 2, for example, without backing plates, had large changes in sample temperature for similar powers. The curves for No.s 3 and 4 show more consistency, and could be used for sample specific temperature prediction.

5.4.7 Surface Structure from LEED

Photographs of LEED patterns were taken over an energy range of 35.1eV to 316.1 eV (Sample 1), 35.3eV to 430.0 eV (Sample 3.) and 34.4eV to 362.8eV (Sample 4.). Their distinct patterns were indicative of a clean surface. However, at energies greater than 180eV, the background intensity increased significantly. The patterns were identified as those of the clean reconstructed Si (2 X 1) surface, resembling those of (39) and (42).

Using the Ewald sphere construction (44,45, Figure 5.12), a value for the reciprocal lattice spacing was obtained from a photograph of the LEED pattern of Sample 1 at 92.4eV, as follows. Spots were first identified on the photograph via an xz coordinate system with its origin at the centre of the outline of the hemispherical grid analyzer (the photograph was assumed to lie on an xz plane). These values were converted to spherical polar coordinates (R,θ,ϕ), R the radius of the hemisphere as measured directly from the photograph. The spot at the origin of the pattern (on the photograph), caused by undiffracted electrons, was defined at $(R,\pi/2,\pi/2)$ radians. Hence for any two spots 1) and 2), their corresponding positions on an Ewald sphere construction were defined as (r,θ_1,ϕ_1) and (r,θ_2,ϕ_2), where $r = 1/\lambda$ was the radius of the Ewald sphere. λ for 92.4eV is 1.28Å, obtained from de Broglie's relation

$$\lambda = h / p \quad \text{or} \quad \lambda = (150 / E)^{1/2} \text{ Å}$$

where E is the energy in eV. The reciprocal lattice spacing between spots was then easily found from

$$s^2 = (z_2 - z_1)^2 + (x_2 - x_1)^2$$

where

$$x_1 = r \sin\theta_1 \cos\phi_1 \qquad z_1 = r \cos\theta_1$$

$$x_2 = r \sin\theta_2 \cos\phi_2 \qquad z_2 = r \cos\theta_2$$

Comparing values to the known Si-Si lattice spacing of 5.43Å, the calculated reciprocal lattice spacing ratio was 1.01 +/- .05, a good agreement.

5.4.8 Reappearance of Contaminants

The silicon, once cleaned, did not stay that way. Auger spectra of Sample No.s 3 and 4 show an increase in carbon and oxygen levels with time. Electron beam heating was used to remove the built-up contaminants. Data concerning the build up and removal of contaminants is given in Table 5.2.

There was a possibility of an increased rate of carbon contamination from exposure to an electron flux (49,50). During the period sample No. 3 was monitored and reheated, at least one of the AES, LEED and SEM electron sources was continuously on. With sample No. 4 all electron sources were off for 22.8 hrs., 24 hrs., 72 hrs., 104 hrs., and 64 hrs.

For No. 4, the 15 W heating removed all of the oxygen and most of the removable carbon. Further heating returned the amount of carbon to the previous "clean" level. There seemed to be no long term carbon build up when sitting with all electron sources off. No evidence of change to thermal contact with the sample was discerned, hence corresponding temperatures for 15 W and 30 W were 700-800°C D.F. and 900-1000°C D.F. respectively. For No. 3, contaminant removal occurred for temperatures of 900 and 1030°C D.F.

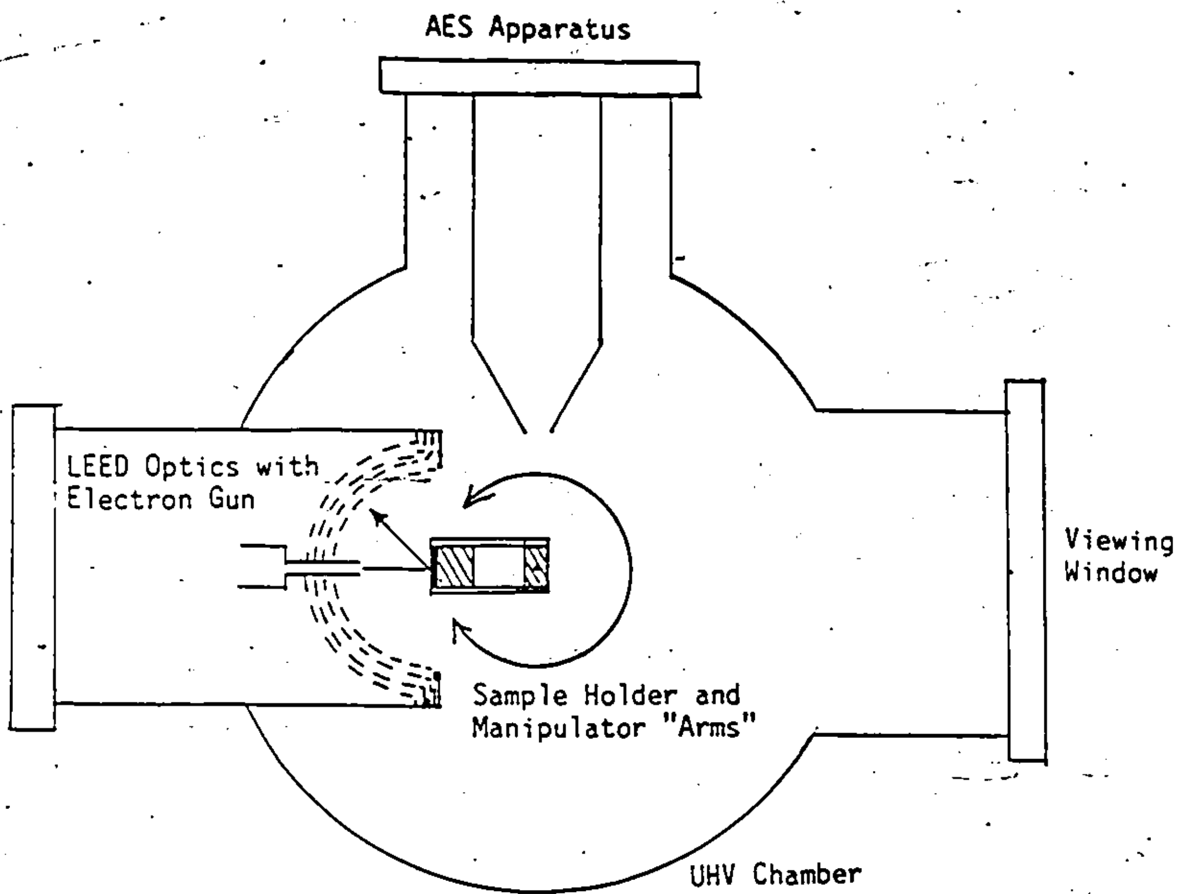

Figure 5.1 LEED Configuration at NRC
(as seen from above)

Figure 5.2 Cylindrical Mirror Analyzer
(from (44))

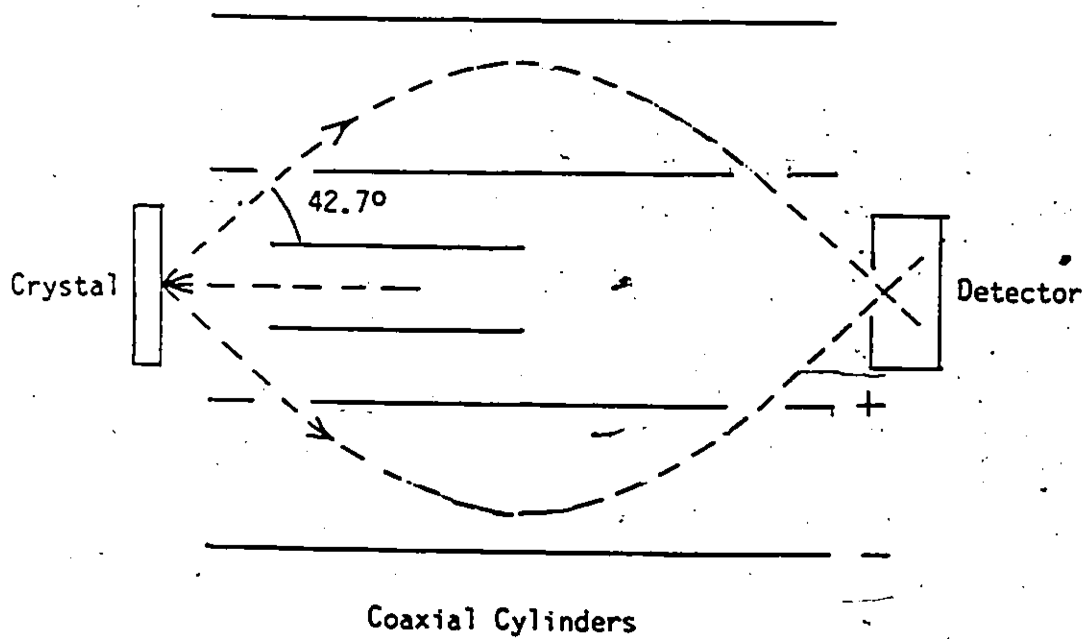

Figure 5.3 Electron Energy Diagram

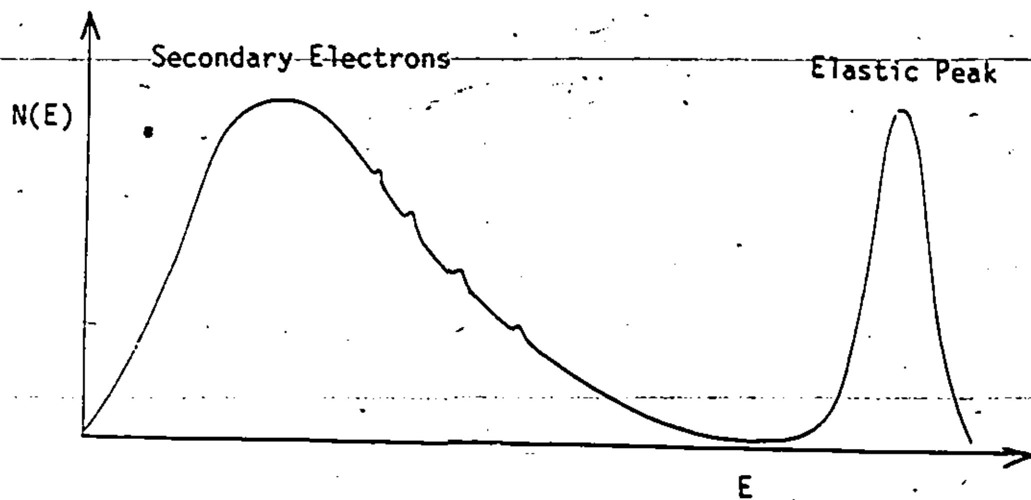

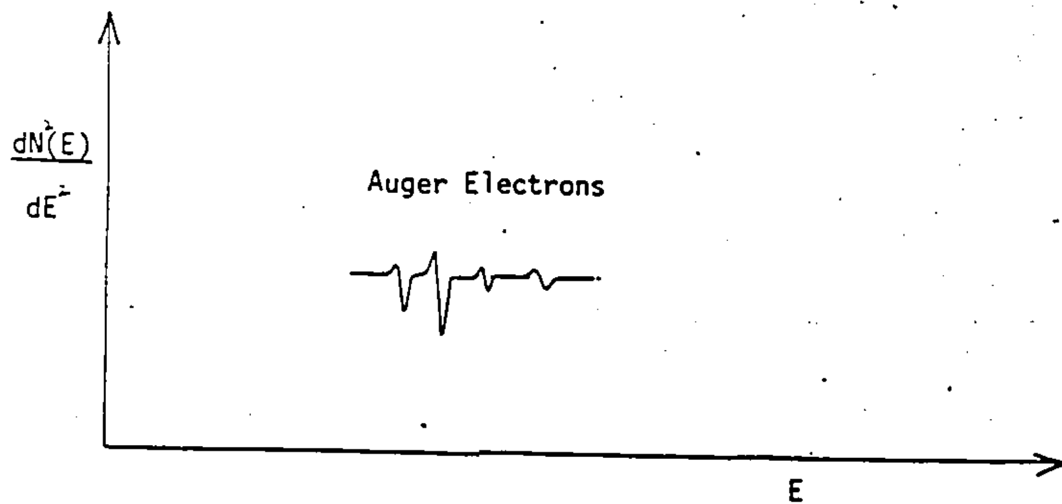

Figure 5.4 Sample Mounting Configuration
a) Sample Holder/Electron Bombarder Block

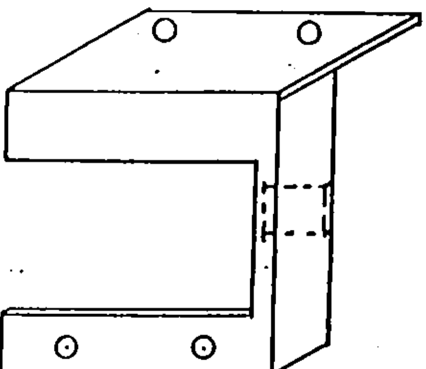

Sample Holder

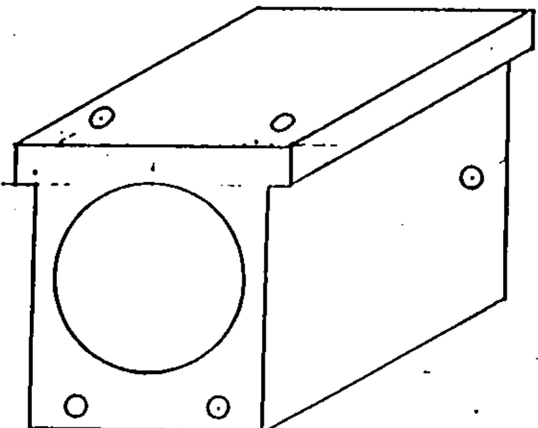

Electron Bombarder Block

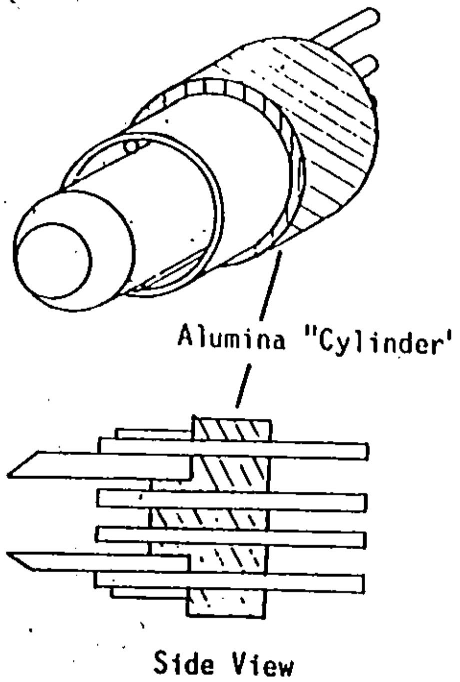

Electron Bombarder

Figure 5.4 Sample Mounting Configuration
b) Sample Mounting Plate

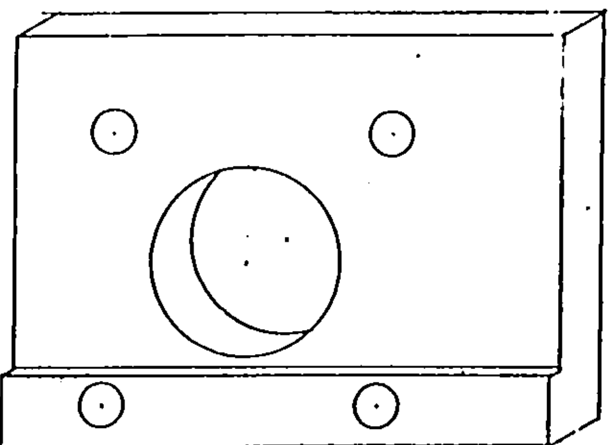

Mounting Plate

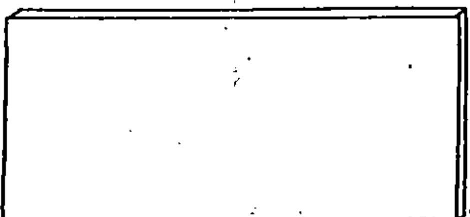

Silicon Wafer Piece
(Molybdenum Backing Plate
of similar dimensions)

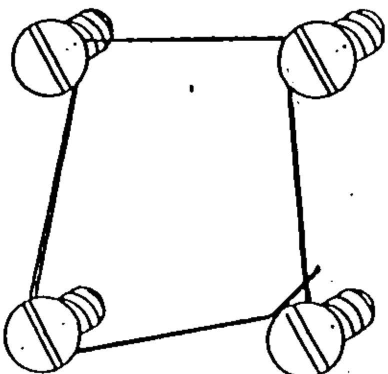

Molybdenum Screws and
Fastening Wire

Figure 5.5 Electron Bombarder Circuit

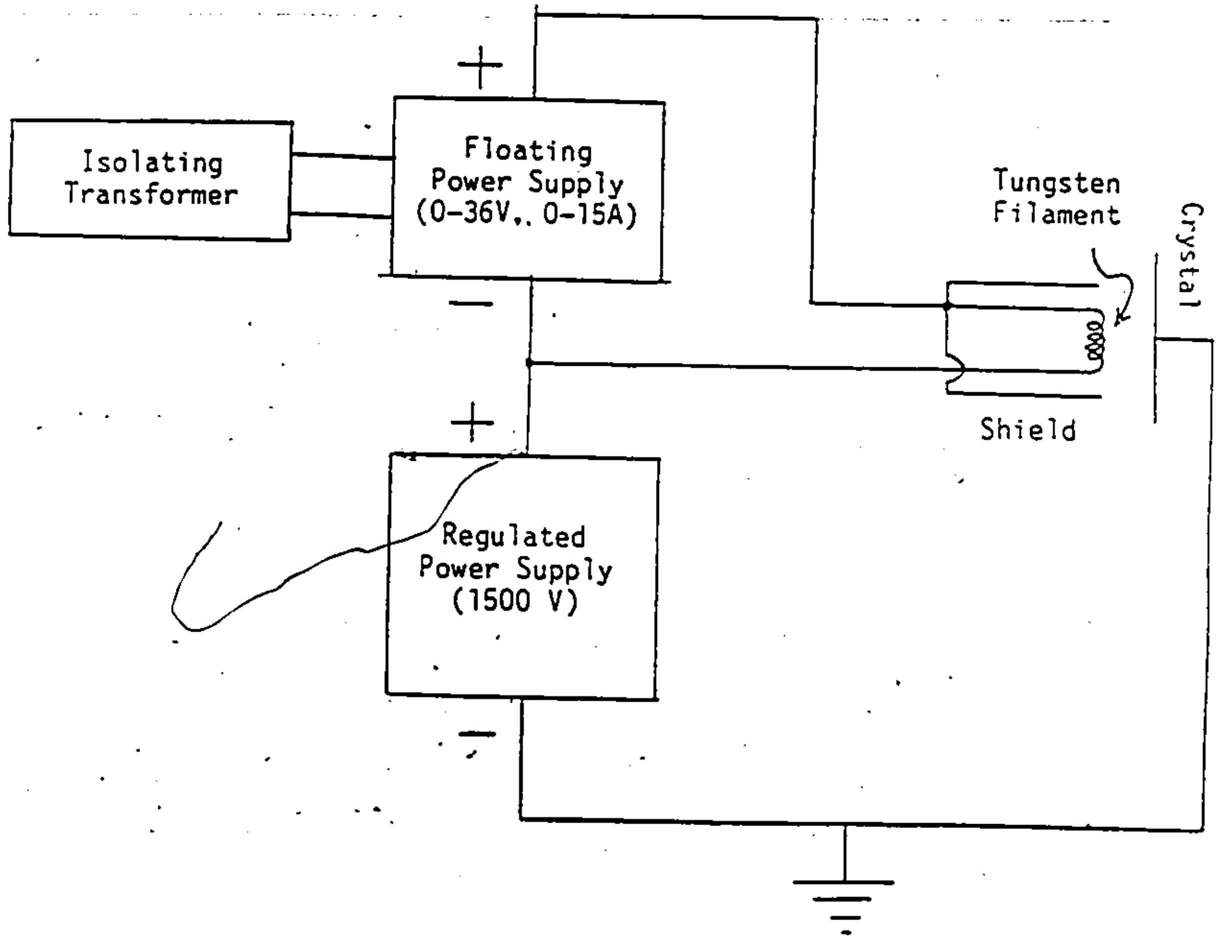

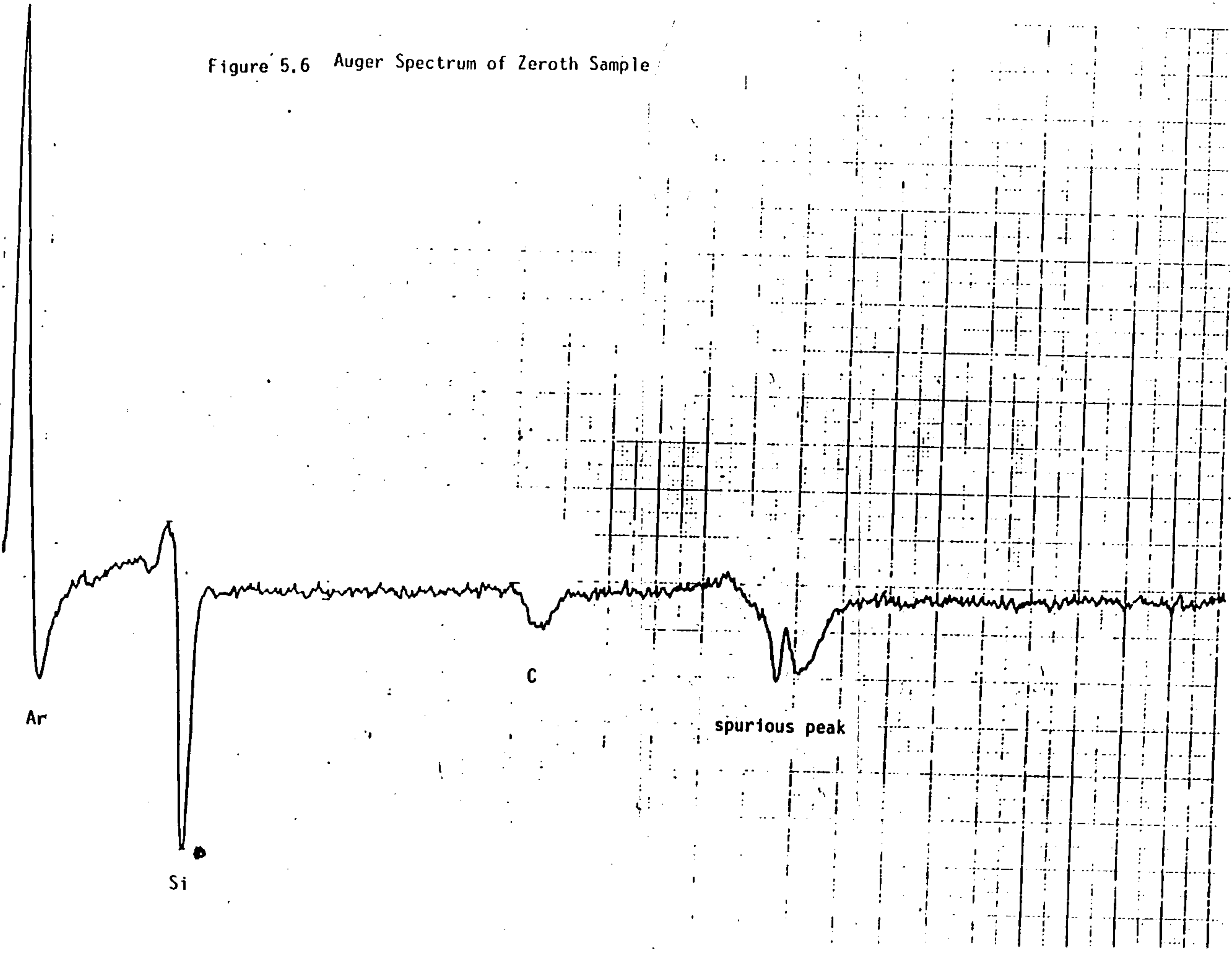

Figure 5.6 Auger Spectrum of Zeroth Sample

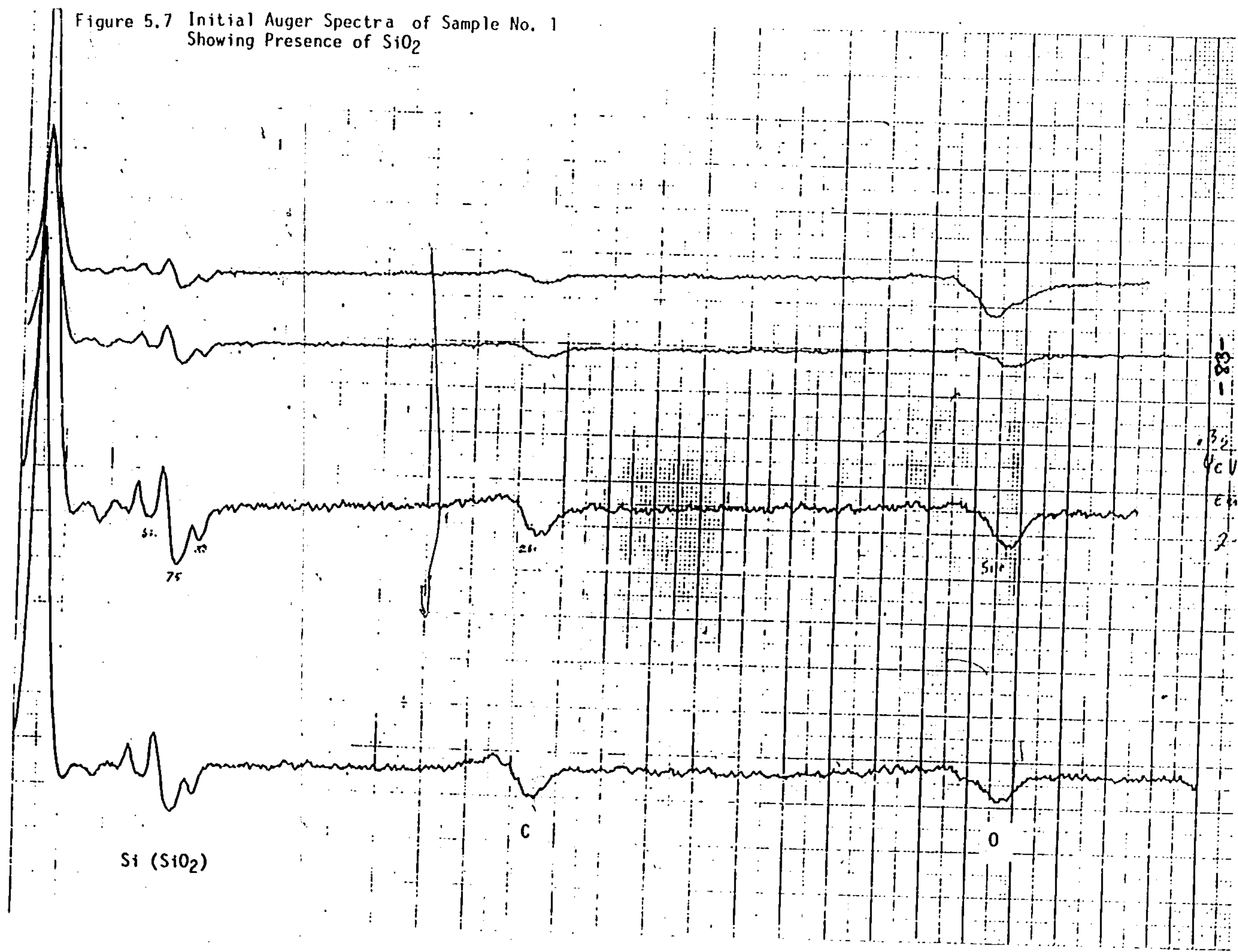

Figure 5.7 Initial Auger Spectra of Sample No. 1 Showing Presence of SiO_2

Figure 5.8 Auger Spectrum of Clean Surface (No. 3)

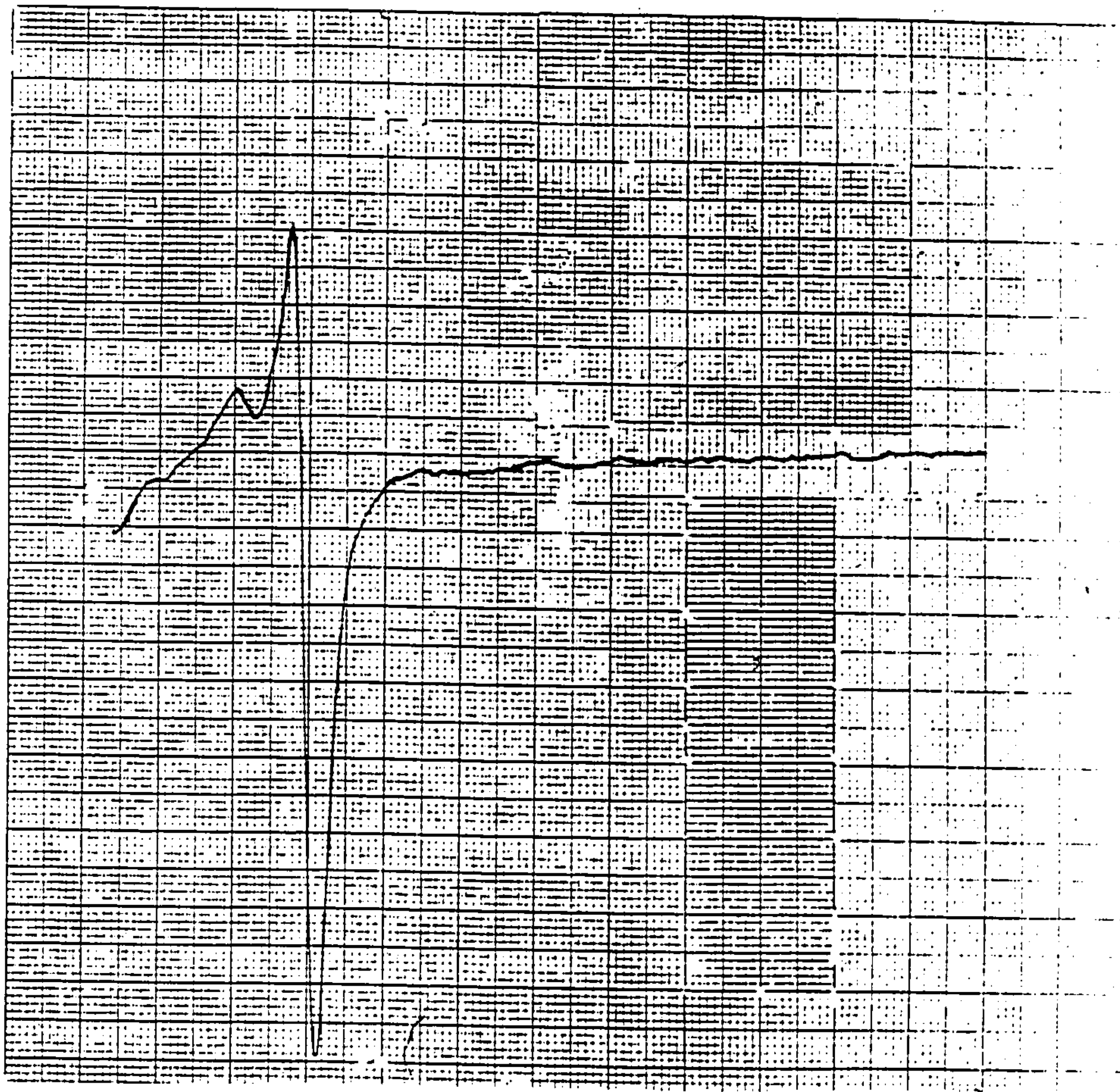

Figure 5.9 Spatial Distribution of Contaminants C and O

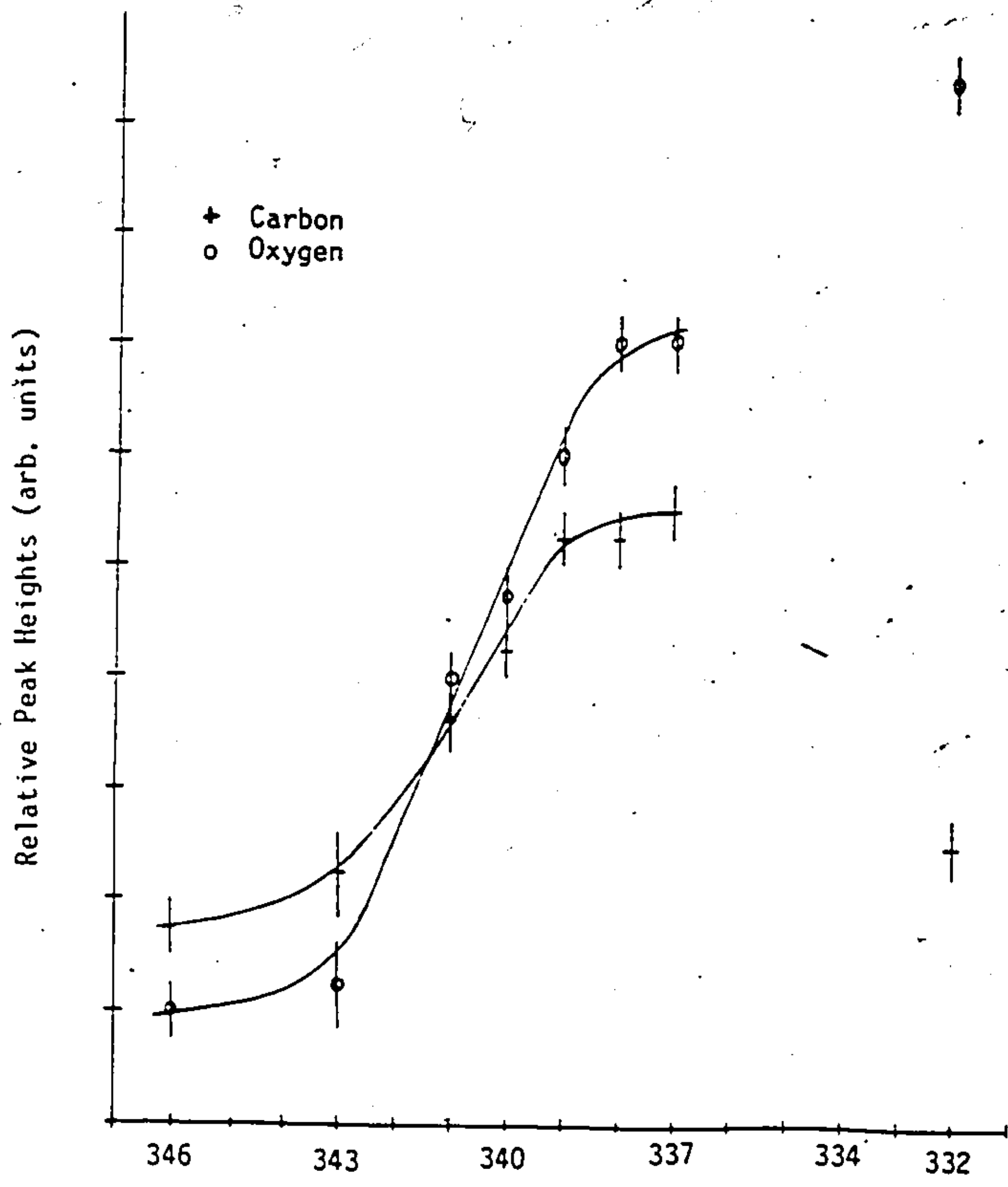

Table 5.1
Summary of Sample Cleaning Measurements

Sample	Location	C/Si	O/Si	Background/Si	Particulars
0	centre	0.14	0.06	0.06	O peak not detected, Ar/Si = 2.0
1	centre	0.4	0.5	0.1	"Before" , P = 2 X 10^{-9} Torr, no backing plate.
	centre edge	0.017 0.16	0.007 0.24	0.007 0.05	O level less than background, after hole appeared
2	centre	0.19	0.54	0.06	"Before", no backing plate
		0.38 0.59 0.54 0.40 0.14 0.14	0.60 0.76 0.46 0.18 0.03 0.03	0.03 0.03 0.08 0.08 0.03 0.03	890°C D.F., 820°C I.R., 4 X 10^{-8} Torr 2 X 10^{-7} Torr, e-guns still operating 980°C D.F., 900°C I.R., 8 X 10^{-8} Torr 1040°C D.F., 940°C I.R., 3 X 10^{-8} Torr 1080°C D.F., 980°C I.R., 3 X 10^{-8} Torr 1140°C D.F., 1000°C I.R., 4 X 10^{-8} Torr, no structure visible with LEED.
3	centre	0.12	0.76	0.04	Boron?/Si = 0.24, "before"
		0.09 0.003	0.51 0.003	0.06 0.003	B?/Si = 0.22, 810°C D.F., 1 X 10^{-9} Torr 900°C D.F., 2.6 X 10^{-9} Torr; LEED pattern obtained, 1.5 X 10^{-10} Torr.
4	centre -2mm	0.07 0.06	0.24 0.14	0.02 0.02	"Before", "before", 1.1 X 10^{-10} Torr (total SEM)
	centre -2mm	0.005 0.009	0.005 0.014	0.005 0.005	C & O levels indistinguishable from background. 990°C D.F.

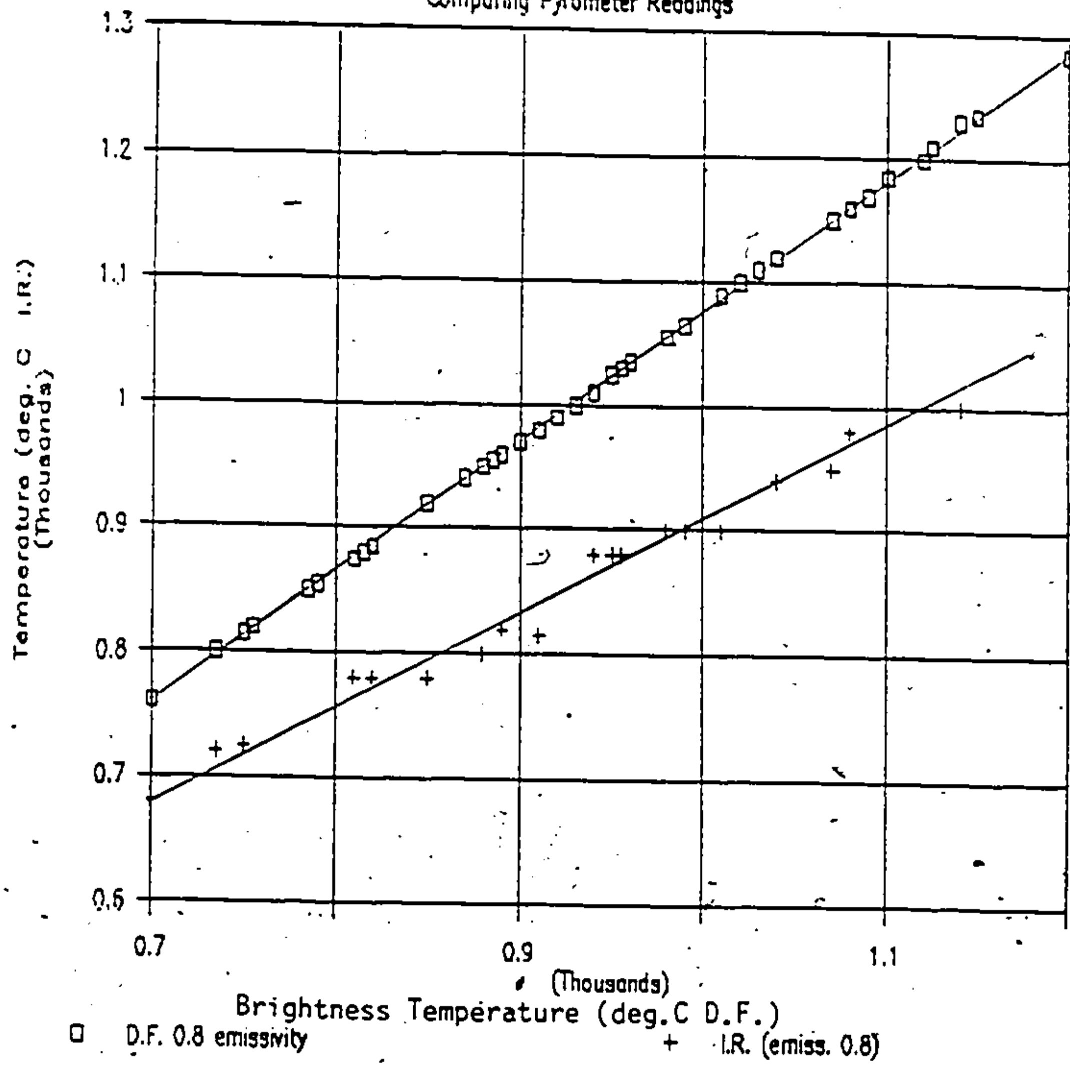
Figure 5.10 Temp. I.R. vs. Temp. D.F.
Comparing Pyrometer Readings
Temperature (deg. C I.R.)
(Thousands)
1.3
1.2
1.1
1
0.9
0.8
0.7
0.6
0.7
0.9
1.1
(Thousands)
Brightness Temperature (deg.C D.F.)
D.F. 0.8 emissivity
I.R. (emiss. 0.8)

Figure 5.11 Relation between Power and Temperature

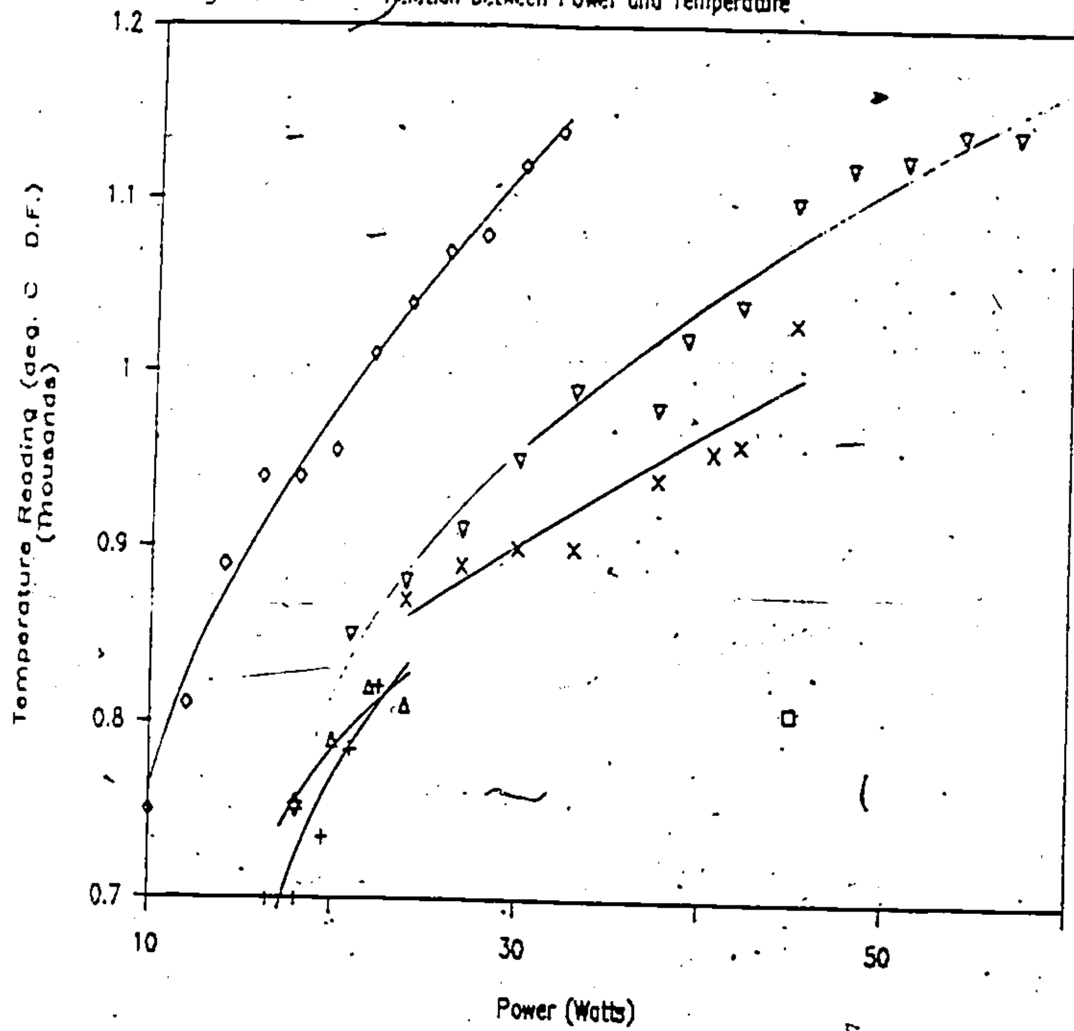

□ Sample No. 1, 1500V supply

\+ No. 2, 1500V supply

◇ No. 2, 1000V supply

△ No. 3, 1000V supply

× No. 3, 1500V supply

▽ No. 4, 1500V supply

Figure 5.12 Ewald Sphere Construction

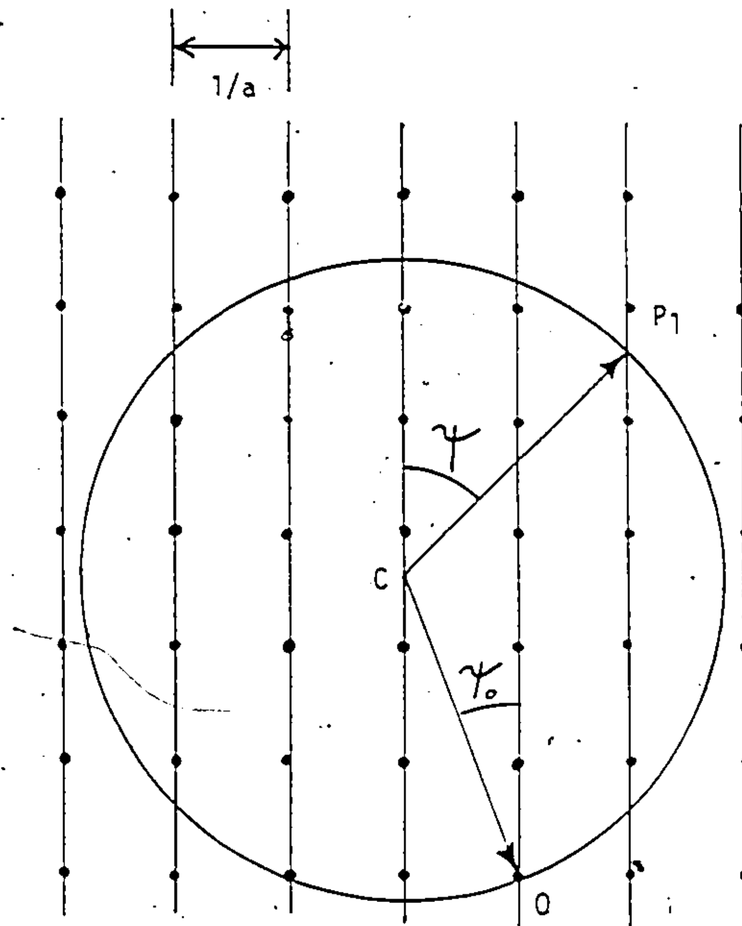

For an angle of incidence ψ_o, diffraction occurs at angles ψ given by

$$1/\lambda \sin \psi = 1/\lambda \sin \psi_o + h\,1/a$$

In the present calculation, $\psi_o = 0$:

O is at $(1/\lambda, 3\pi/2, \pi/2)$,

P_1 at $(1/\lambda, \theta_1, \phi_1)$.

At LEED energies diffraction is limited to surface and near-surface atoms, hence LEED mostly "sees" the 2-dimensional surface lattice, while deeper layers, evidence of a 3-dimensional lattice, are not probed. The 2-dimensional reciprocal lattice is visualized when a triperiodic lattice is extended along one of its axes. Since distances in reciprocal space are inversely proportional to distances in real space, the reciprocal lattice points merge into a set of parallel rods which pass through the lattice points of the reciprocal surface net.

Table 5.2 Reappearance of Contaminants

Sample	Time Elapsed	Process	C/Si	O/Si	Noise/Si	Comment
3.	0 hrs		0.003	0.003	0.003	Sample just cleaned
	2 hrs		0.14	0.05	0.01	e-guns on
	1 hr		0.46	0.025		B/Si = 0.021
	20 min.	900°C D.F.	0.016	0.009	0.009	6 X 10^{-10} Torr
	1 hr. 20 min.	1030°C D.F.	0.013	0.006	0.006	
	after		0.030	0.007		AES gun on since previous scan.
4	0 hrs	Heating	0.014	0.010		
	0.05 hrs	Heating repeated	0.011	0.015		
	0.9 hrs	None	0.011			
	0.03 hrs	Heating, 20W	0.010	gone		
	0.20 hrs	None	0.009			
	22.8 hrs	None	0.015	0.005		
	0.30 hrs	15W: 10mA, 1500V	0.007	gone		Heating 15W is enough to remove O signal & reduce C signal 2 X.
	24 hrs	None	0.016	0.009		
		15W	0.010	gone		
	0.9 hrs	30W: 20mA, 1500V	0.009	gone		
	72hrs	None	0.014	0.006		
		15W	0.011	gone		
		30W	0.008	gone		The 15W heating removed all the O & most of the removable C. Further heating returned C to the previous level.
	104hrs	None	0.022	0.063		
	64hrs	None	0.024	0.008		
		None	0.03	0.009		Second AES scan

6.0 Conclusions and Recommendations

6.1 Conditions for Clean Si(100)

The Si(100) samples were considered to be clean once the measured contaminant levels had dropped to C/Si = 0.017 and O/Si = 0.007. In most cases the C/Si ratio was better than this (i.e. < 0.017) and the O/Si ratio indistinguishable from background.

The minimum condition for successful cleaning was the combination of 900°C D.F. and 2.6 X 10^{-9} Torr. Cleaning did not take place for pressures higher than 8 X 10^{-8} Torr, even when the sample was heated to 1140°C D.F. The largest surface area cleaned occurred for pressures in the 10^{-10} Torr range.

Each time a sample was cleaned, a clear LEED (2 X 1) pattern was easily obtained. There occurred no instances of either a dirty sample and a good LEED image or of a clean sample with a poor LEED image.

A number of experimental conditions facilitated the cleaning of samples. The replacement of the benders with vacuum fired plates, able to take high temperatures without outgassing, improved vacuum conditions in the proximity of the sample. The presence of a backing plate maintained a consistent thermal contact for reproducible sample heating. Extensive outgassing by running the electron guns for many hours beforehand and by running the electron bombarder for a few hours beforehand, at a temperature not higher than 850°C, improved vacuum conditions as well as removing some of the oxide. Maintaining sample cleanliness was

facilitated by sitting with all electron sources off; there seemed to be no long term carbon build-up.

A number of experimental conditions did not seem to adversely affect results. One instance was the delay of 5 hours before loading the ozone treated sample into the UHV chamber. During this time the entire manipulator system was also exposed to air. This point is favourable for the successful shipment of ozone prepared samples to the University of Ottawa. Contaminant build-up was faster while the electron sources were operating, but recleaning was possible for samples contaminated at 6 X 10^{-10} Torr for less than 3 hours.

6.2 Baking Procedure

Baking the UHV apparatus at the University of Ottawa has been shown to be of prime importance in order to achieve an optimum environment for the preparation and maintainance of clean samples. Baking to 200°C overnight improved the pressure in the differential pumping chamber to 7.4 X 10^{-10} Torr, from 9.5 X 10^{-9} Torr. A similar vacuum improvement is expected after baking the sealed sample chamber.

To reduce difficulties with high pressures and outgassing in the sample chamber during sample cleaning, it is recommended that the sample chamber is baked at least once, before sample mounting. This will require the achievement of pressures less than 10^{-10} Torr, followed by backfilling the chamber with (dry) nitrogen or argon, followed by briefly

opening the chamber and installing the prepared sample.

The triac-oven controller circuit successfully reduced the number of potentiometer settings needed to achieve the desired baking temperature. A steady state temperature near 200°C was obtained at the "40% power" setting. Experience will assist in optimizing the baking procedure further. In addition, the controller circuit will allow the implemention of computer control of the baking temperature, via a logic input to the triac gate.

6.3 Surface Scattering Experiment Considerations

The apparatus and procedure have been developed, whereby clean samples of Si(100) can be prepared and maintained in an ultrahigh vacuum facility, into which keV ions can readily be directed for ion- surface studies, specifically, for surface scattering at grazing incidence.

The surface scattering experimental apparatus is capable of achieving UHV experimental conditions, with baking. The baking oven has successfully survived testing and contributes to improved vacuum conditions. The bakeout oven can be easily managed by one person.

With respect to the scattering geometry, the support table supports the beam line in the correct alignment and allows changes in alignment. The rotating platform will allow the changing of detector angles. Directions of random alignment, at grazing incidence, will be selected

experimentally through rotation of the goniometer. The area of clean surface will limit the size of the "scattering window". One wants to detect only scattered ions from the cleaned part of the sample. A maximum diameter of 4mm was cleaned, from the surface cleaning procedure at NRC.

The minimum standard set for vacuum and temperature was 900°C D.F., (the brightness temperature as measured by the disappearing filament pyrometer at NRC), and 2.6 X 10^{-9} Torr. It is recommended to use the NRC pyrometers to calibrate the electron beam heater at the University of Ottawa. The oxidized sample can be safely transported from the NRC ozone reactor and installed in the surface scattering sample chamber, ready for cleaning. For better thermal distribution across the sample during cleaning, it is recommended a backing plate be used between the electron bombarder and the sample. Prolonged outgassing of electron sources prior to cleaning sample (at < 850°C) is also recommended. Sample cleanliness can be maintained by periodic electron bombardment, as was established at NRC.

References

1. H.H. Brongersma, N. Hazewindus, J.M. van Nieuwland, A.M.M. Otten, and A.J. Smets, Rev. Sci. Instrum., Vol. 49 No. 6 June 1978

2. G. Holmen, E. Kugler, O. Almen, Nucl. Inst. and Meth. 105 (1972) 545-550

3. J.P. Hobson, Surface and Colloid Science, Vol.11, ed. R.J. Good, R.R. Stromberg, Plenum, 1979, 187-215.

4. W.T. Moore, Ph.D. Thesis, University of British Columbia, 1981

5. T.M. Buck, G.H. Wheatley, Surf. Sci. 33 (1972) 35-55

6. D.J. Ball, T.M. Buck, D. Macnair, G.H. Wheatley, Surf. Sci. 30 (1972) 69-90.

7. T.M. Buck, Y.-S. Chen, G.H. Wheatley, W.F. van der Weg, Surf. Sci. 47 (1975) 244-255

8. W.C. Turkenburg, Ph.D. Thesis, 1976, U. Amsterdam

9. J.F. van der Veen, Surf. Sci. Reports 5 (1985) 199-288

10. M. Aono, Y.Hou, C. Oshima, Y. Ishizawa, Phys. Rev. Lett. Vol. 49, No. 8, 23 August 1982, 567-570

11. H. Niehus, Surf. Sci. 166 (1986) L107-L110

12. W.C. Turkenburg, B.G. Colenbrander, H.H. Kersten, F.W. Saris, Surf. Sci. 47 (1975) 272-281

13. T.M. Buck, G.H. Wheatley and L.C. Feldman, Surf. Sci. 35 (1973) 345-361

14. H. Winter, R. Zimny, A. Schirmacher, B. Becker, H.J. Andrä, R. Fröling, Z. Phys. A 311, 267-280 (1983)

15. C. Sitter, J.A. Davies, T.E. Jackman, and P.R. Norton, Rev. Sci. Instrum. 53(6), Jun. 1982

16. E.P. Suurmeijer, A.L. Boers, Surf. Sci. 43 (1973) 309-352

17. W. Graser, C. Varelas, Physica Scripta, Vol. T6, 153-163, 1983

18. H.J. Andrä, H. Winter, R. Fröling, N. Kirchner, H.J. Plöhn, W. Wittmann, W. Graser, and C. Varelas, Nucl. Inst. & Meth. 170 (1980) 527-538

19. H. Akazawa, I. Kusonoki, Y. Murata, Surf. Sci. 177 (1986) 577-592

20. J. Lindhard, Mat. Fys. Medd. Dan. Vid. Selsk. 34, no. 14 (1965)

21. L.F. de Ferrariis, R.A. Bargiola, Phys. Rev. A 33, #6 June 1986, 4449-4451

22. A.I. Dodonov, Sh.N. Garin, E.S. Mashkova, V.A. Molchanov, Surf. Sci. 140 (1984) L244-L252

23. J.N.M. van Wunnik, J.J.C. Geerlings, J. Los, Surf. Sci. 131 (1983) 1-16

24. G.A. Somorjai, Chemistry in Two Dimensions: Surfaces, Cornell University Press, Ithaca, 1981

25. S. Tougaard, P. Morgen, J. Onsgaard, Surf. Sci. 111 (1981) 541-554

26. F. Reif, Fundamentals of Statistical and Thermal Physics, McGraw-Hill 1965, 270-273.

27. Y.S. Chen, G.L. Miller, G.A.H. Robinson, G.H. Wheatley, T.M. Buck, Surf. Sci. 62 (1977) 133-147

28. S. Willerding, H. Steininger, K.J. Snowdon, W. Heiland, Nucl. Inst. and Meth. B2 (1984) 453-456

29. G.J. Kelly, Master's Thesis, University of Ottawa, 1987

30. J. Lipkowski, U. of Guelph, private communication, 1986

31. A. Roth, Vacuum Technology, 2nd, revised ed., N. Holland 1982

32. G.F. Weston, Ultrahigh Vacuum Practice, Butterworth & Co. 1985.

33. Buchsbaums's Complete Handbook of Practical Electronic Reference Data, Prentice-Hall, 1973.

34. R. Hull, J.C. Bean, J.M. Gibson, D.C. Joy and M.E. Twigg, MBE Proceedings *

35. R.W. Hardeman, D.J. Robbins, D.B. Gasson, A. Daw, MBE Proceedings *

36. M. Tabe, Appl. Phys. Lett. 45 (10) 15 Nov. 1984, pp. 1073

37. A. Ishizaka, K. Nakagawa, Y. Shiraki, Collected paper of MBE-CST-2, 1982, Tokyo, A-10-2

38. Y. Mikata, T. Inoue, S. Takasu, T. Usami, T. Ohta, H. Hirano pp.45 *

39. L.C. Feldman, P.J. Silverman, I. Stensgaard, Nucl. Instr. & Meth. 168 (1980) 589-593

40. R.M. Tromp, R.G. Smeenk, F.W. Saris, D.J. Chadi, Surf. Sci. 133 (1983) 137-158

41. T.D. Poppendieck, T.C. Ngoc, M.B. Webb, Surf. Sci. 75 (1978) 287-315

42. A. Ignatiev, F. Jona, M. Debe, D.E. Johnson, S.J. White, D.P. Woodruff, Phys. C: Solid State Phys., Vol. 10, 1977

43. R.M. Tromp, R.G. Smeenk, F.W. Saris, Phys. Rev. Lett. Vol. 46 No. 14 6 April 1981 pp. 939

44. M. Prutton, Surface Physics, 2nd ed., Oxford University Press, Oxford OX2 6DP, 1983

45. P.J. Estrup, E.G. McRae, Surf. Sci. 25 (1971) 1-52

46. B. Carriere, A. Chouiyakh, B. Lang, Surf. Sci. 126 (1983) 495-501

47. P.W. Palmberg, G.E. Riach, R.E. Weber, N.C. MacDonald, Handbook of Auger Electron Spectroscopy, Physical Electronics Industries Inc., 1972.

48. F.W. Sears, Optics, 3rd ed., Addison-Wesley 1958, pp. 316.

49. E. Ekwelundu, A. Ignatiev, Surface Science 179 (1987) 119-131

50. S. Tougaard, P. Morgen, J. Onsgaard, Surface Science 111 (1981) 545-554

* obtained through the invaluable assistance of Mike Denhof, NRC.